ETH
Eidgenössische Technische Hochschule Zürich
Swiss Federal Institute of Technology Zurich

Multigrid Solver for Boundary Value Problems for the Dirac Operator

Master Thesis

Radovan Dabetić

Thursday 11th September, 2025

Advisors: Prof. Dr. R. Hiptmair
D-MATH, ETH Zürich

Abstract

In this thesis, we address the boundary value problem for the Hodge-Dirac operator on a bounded, Lipschitz, polytopal, and topologically trivial domain $\Omega \subset \mathbb{R}^n$. Utilizing a geometric multigrid method, we solve the resulting system of linear equations derived from finite element exterior calculus (FEEC) and discrete exterior calculus (DEC) discretizations.

The assembly and analysis of Galerkin matrices for structured grids are presented, with the "Dirac$^2 = -\Delta$" property verified in the discrete setting. This facilitates the development and evaluation of appropriate smoothers, transforming smoothers (more specifically, distributive relaxation), in both two- and three-dimensional cases.

Unstructured grids are also discussed, and under relatively mild conditions we prove a Poincaré inequality for DEC, stability of DEC, and ultimately spectral equivalence between FEEC and DEC. We elucidate a multigrid approach for DEC validated through numerical testing in 2D and 3D. Based on the DEC smoother, a smoother for the FEEC problem is constructed and tested in 2D, showing robust rates of convergence.

Furthermore, convergence of DEC is proven under the assumption of a well-centered mesh and a sufficiently regular solution, which is demonstrated using numerical tests in 2D.

Acknowledgments

I want to thank Prof. Dr. Ralf Hiptmair for his supervision and fruitful discussions during this project. My thanks also go to Wouter Tonnon for giving me tips on the code and recommending I try out `MFEM`.

I would also like to thank my family for supporting me throughout my studies.

Contents

List of Abbreviations

DEC Discrete Exterior Calculus

DGSR Distributive Gauss-Seidel Relaxation

DOF Degree of Freedom

FEEC Finite Element Exterior Calculus

Symbols

$\operatorname{tril}(A)$	The lower triangular part of the matrix A
$\Lambda^k(\Omega)$	Space of smooth differential k-forms on Ω
$L^2\Lambda^k(\Omega)$	Space of differential k-forms with coefficients in L^2
$L^2\Lambda(\Omega)$	Exterior algebra of L^2-differential forms
$H\Lambda^k(\Omega)$	Space of differential k-forms in $L^2\Lambda^k(\Omega)$ with weak exterior derivative
$H\Lambda(\Omega)$	Exterior algebra of differential forms in $L^2\Lambda(\Omega)$ with weak exterior derivative
$H^*\Lambda^k(\Omega)$	Space of differential k-forms in $L^2\Lambda^k(\Omega)$ with weak codifferential
$H^*\Lambda(\Omega)$	Exterior algebra of differential forms in $L^2\Lambda(\Omega)$ with weak codifferential
$\mathring{H}\Lambda^k(\Omega)$	Forms in $H\Lambda^k(\Omega)$ with zero trace
$\mathring{H}\Lambda(\Omega)$	Space of elements in $H\Lambda(\Omega)$ with zero trace
$\star_k$	Hodge star on k-forms
d^k	Exterior Derivative on k-forms
δ_k	Codifferential on k-forms
d	$0 \oplus \bigoplus_k d^k$
δ	$\bigoplus_k \delta_k \oplus 0$
D	Hodge-Dirac operator on differential forms
$L^2_*\Lambda^n(\Omega)$	Space of n-forms in $L^2\Lambda^n(\Omega)$ with zero mean
$\mathring{\mathfrak{V}}$	$\bigoplus_{k=0}^{n-1} \mathring{H}\Lambda^k(\Omega) \oplus L^2_*\Lambda^n(\Omega)$
V_k^h	Space of Whitney k-forms
V^h	$\bigoplus_k V_k^h$
$\mathring{V}_k^h$	$V_k^h \cap \mathring{H}\Lambda^k(\Omega)$, space of elements in V_k^h with zero trace
$\mathring{V}^h$	$V^h \cap \mathring{\mathfrak{V}}$, space of elements in V^h with zero trace or zero mean in the case of n-forms
A^{FEEC}	FEEC Galerkin matrix
$\mathrm{M}_k^{\mathrm{FEEC}}$	Mass matrix of $\mathring{V}_k^h$
$\mathrm{M}^{\mathrm{FEEC}}$	Mass matrix of $\mathring{V}^h$
$\mathcal{T}$	(Conforming) Simplicial mesh of the computational domain
$C^k(\mathcal{T})$	Space of k-cochains on $\mathcal{T}$

$\mathring{C}^k(\mathcal{T})$	Space of k-cochains on $\mathcal{T}$ with zero on the boundary
$C(\mathcal{T})$	$\bigoplus_k C^k(\mathcal{T})$
$\mathcal{W}^k$	Whitney map on k-cochains on $\mathcal{T}$
$\mathcal{W}$	$\bigoplus_k \mathcal{W}^k$
$C^n_*(\mathcal{T})$	Space of n-cochains w on $\mathcal{T}$ with $\sum_{\sigma\in\mathcal{T}^n}\langle \mathsf{w},\sigma\rangle = 0$
$\mathring{C}(\mathcal{T})$	$\bigoplus_{k=0}^{n-1}\mathring{C}^k(\mathcal{T})\oplus C^n_*(\mathcal{T})$
$\mathcal{R}^k$	De Rham map on k-forms
$\mathcal{R}$	$\bigoplus_k \mathcal{R}^k$
∂^k	Coboundary operator on $C^k(\mathcal{T})$
$\mathrm{d}^{\mathrm{DEC}}$	$0\oplus\bigoplus_{k=0}^{n-1}\partial^k$
$\star_k$	DEC Hodge star, see Definition 3.6
δ_k^{DEC}	DEC Codifferential $\delta_{k+1}^{\mathrm{DEC}} := (-1)^{k+1}\star_k^{-1}\tilde{\partial}^{n-(k+1)}\star_{k+1}$, where $\tilde{\partial}^{n-(k+1)}$ denotes the coboundary operator on $C^{n-(k+1)}(\tilde{\mathcal{T}})$
δ^{DEC}	$\bigoplus_{k=1}^{n}\delta_k^{\mathrm{DEC}}\oplus 0$
$[\![\cdot,\cdot]\!]_k$	DEC inner product on $C^k(\mathcal{T})$
$[\![\cdot,\cdot]\!]$	DEC inner product on $C(\mathcal{T})$, $[\![\cdot,\cdot]\!] := \sum_k [\![\cdot_k,\cdot_k]\!]_k$
$\lvert\!\lvert\!\lvert\cdot\rvert\!\rvert\!\rvert$	Norm induced by $[\![\cdot,\cdot]\!]$
$[\![\cdot,\cdot]\!]_{H\Lambda(\Omega)}$	$[\![\cdot,\cdot]\!] + \left[\!\!\left[\mathrm{d}^{\mathrm{DEC}}\cdot,\mathrm{d}^{\mathrm{DEC}}\cdot\right]\!\!\right]$
$\lvert\!\lvert\!\lvert\cdot\rvert\!\rvert\!\rvert_{H\Lambda(\Omega)}$	Norm induced by $[\![\cdot,\cdot]\!]_{H\Lambda(\Omega)}$
$\mathrm{M}_k^{\mathrm{DEC}}$	Mass matrix of $\mathring{C}^k(\mathcal{T})$ with $[\![\cdot,\cdot]\!]_k$ as the inner product
$\mathrm{M}^{\mathrm{DEC}}$	Mass matrix of $\mathring{C}(\mathcal{T})$ with $[\![\cdot,\cdot]\!]$ as the inner product
A^{DEC}	$\mathrm{M}^{\mathrm{DEC}}\mathrm{D}^{\mathrm{DEC}}$ "DEC-mass-lumped Galerkin matrix"

Chapter 1

Hodge-Dirac Operators

1.1 Exterior Calculus

We will now very briefly introduce some notation and concepts from exterior calculus. For more details, refer to [9, 2, 12, 22]. The following notations are based on [12]. Let $\Omega \subset \mathbb{R}^n$ be a bounded, Lipschitz, polytopal, and *topologically trivial* domain and we write $\Lambda^k(\Omega)$ for the space of smooth k-forms thereon. As in [12] the exterior derivative operators are denoted by $d^k : \Lambda^k(\Omega) \to \Lambda^{k+1}(\Omega)$, $0 \leq k < n$, the (Euclidean) Hodge star operators by $\star_k$ and the codifferential operators by $\delta_k := (-1)^k \star_{k-1}^{-1} d^{n-k} \star_k : \Lambda^k(\Omega) \to \Lambda^{k-1}(\Omega), k = 1, \ldots, n$. The Hodge star operators induce inner products on $\Lambda^k(\Omega)$.

Definition 1.1
The L^2 inner product on two k-forms ω and μ is given by

$$\langle \omega, \mu \rangle_{L^2\Lambda^k(\Omega)} := \int_\Omega \omega \wedge \star_k \mu, \quad \omega, \mu \in \Lambda^k(\Omega).$$

We denote by $\Lambda(\Omega) := \bigoplus_{k=0}^n \Lambda^k(\Omega)$ the exterior algebra of (smooth) differential forms on Ω and write

$$\mathrm{d} := \begin{pmatrix} 0 & & & \\ d^0 & 0 & & \\ & d^1 & 0 & \\ & & \ddots & \ddots \end{pmatrix}, \quad \delta := \begin{pmatrix} 0 & \delta_1 & & \\ & 0 & \delta_2 & \\ & & 0 & \ddots \\ & & & \ddots \end{pmatrix} \tag{1.1}$$

for the exterior derivative and codifferential on $\Lambda(\Omega)$. We equip $\Lambda(\Omega)$ with the natural Hilbert space structure by combining the inner products from Definition 1.1. For $\mathfrak{u} \equiv (u_0, \ldots, u_n), \mathfrak{v} \equiv (v_0, \ldots, v_n) \in \Lambda(\Omega)$ we set

$$\langle \mathfrak{u}, \mathfrak{v} \rangle_{L^2\Lambda(\Omega)} := \sum_{k=0}^n \langle u_k, v_k \rangle_{L^2\Lambda(\Omega)} .$$

Write $L^2\Lambda(\Omega) := \bigoplus_{k=0}^n L^2\Lambda^k(\Omega)$, where $L^2\Lambda^k(\Omega)$ is the space of square-integrable k-forms, i.e. k-forms with coefficients in $L^2(\Omega)$.

Also refer to [2, Section 6.2.6], where Sobolev spaces of differential forms are introduced. Let

$$H\Lambda(\Omega) := \left\{ \mathfrak{u} \in L^2\Lambda(\Omega) : \mathrm{d}\mathfrak{u} \in L^2\Lambda(\Omega) \right\},$$

and define $\mathring{\mathfrak{V}} := \bigoplus_{k=0}^{n-1} \mathring{H}\Lambda^k(\Omega) \oplus L^2_*\Lambda^n(\Omega)$, where

$$L^2_*\Lambda^n(\Omega) := \left\{ \omega \in L^2\Lambda^n(\Omega) : \int_\Omega \omega = 0 \right\}, \tag{1.2}$$

and $\mathring{H}\Lambda^k(\Omega)$ is the space of functions in $H\Lambda^k(\Omega)$ with vanishing trace on $\partial\Omega$, see [2, Section 6.2.6]. Also let $H^*\Lambda(\Omega)$ be the domain of δ, see also [2, Section 6.2.6].

Definition 1.2 ([19, Section 2.1])
We denote the inner product on $H\Lambda(\Omega)$ by

$$\langle \mathfrak{u}, \mathfrak{v} \rangle_{H\Lambda(\Omega)} := \langle \mathfrak{u}, \mathfrak{v} \rangle_{L^2\Lambda(\Omega)} + \langle \mathrm{d}\mathfrak{u}, \mathrm{d}\mathfrak{v} \rangle_{L^2\Lambda(\Omega)}.$$

Definition 1.3
The Hodge-Dirac operator is $\mathrm{D} := \mathrm{d} + \delta$ with domain of definition $\mathcal{D}(\mathrm{D}) := \mathring{H}\Lambda(\Omega) \cap H^*\Lambda(\Omega)$, where the domain of d is $\mathring{H}\Lambda(\Omega)$ and that of δ is $H^*\Lambda(\Omega)$.

Remark 1.4 *There is a connection between the Hodge-Dirac operator we see here and the one from physics, at least in 3D. See Appendix B for more.*

1.2 Variational Problem

Taking the cue from [19] we put the focus on the following boundary value problem[1] for the Dirac operator: Given $\mathfrak{f} \in L^2\Lambda(\Omega)$, seek $\mathfrak{u} \in \mathcal{D}(\mathrm{D}) \cap (\ker \mathrm{D})^\perp, \mathfrak{p} \in \ker \mathrm{D}$ such that

$$\mathrm{D}\mathfrak{u} + \mathfrak{p} = \mathfrak{f}. \tag{1.3}$$

Corollary 8 of [19] establishes the well-posedness and stability of the following weak form of (1.3): Given $\mathfrak{f} \in L^2\Lambda(\Omega)$, seek $\mathfrak{u} \in \mathring{H}\Lambda(\Omega), \mathfrak{p} \in \ker \mathrm{D}$ such that

$$\begin{aligned} \langle \mathrm{d}\mathfrak{u}, \mathfrak{v} \rangle_{L^2\Lambda(\Omega)} + \langle \mathfrak{u}, \mathrm{d}\mathfrak{v} \rangle_{L^2\Lambda(\Omega)} + \langle \mathfrak{p}, \mathfrak{v} \rangle_{L^2\Lambda(\Omega)} &= \langle \mathfrak{f}, \mathfrak{v} \rangle_{L^2\Lambda(\Omega)} \quad && \forall \mathfrak{v} \in \mathring{H}\Lambda(\Omega) \\ \langle \mathfrak{u}, \mathfrak{v} \rangle_{L^2\Lambda(\Omega)} &= 0 && \forall \mathfrak{v} \in \ker \mathrm{D}. \end{aligned} \tag{1.4}$$

As we are working with a domain with trivial topology, $\ker \mathrm{D}$ (the space of harmonic forms) is trivial (see [2, Section 4.3] for more information) except for constant n-forms, i.e. $\ker \mathrm{D}|_{\mathring{\mathfrak{V}}} = \{0\}$, so that we can consider the following simpler problem:

Main Variational Problem

Given $\mathfrak{f} \in L^2\Lambda(\Omega)$ with $\int_\Omega f_n = 0$[a], seek $\mathfrak{u} \in \mathring{\mathfrak{V}}$ such that

$$\mathcal{A}(\mathfrak{u}, \mathfrak{v}) := \langle \mathrm{d}\mathfrak{u}, \mathfrak{v} \rangle_{L^2\Lambda(\Omega)} + \langle \mathfrak{u}, \mathrm{d}\mathfrak{v} \rangle_{L^2\Lambda(\Omega)} = \langle \mathfrak{f}, \mathfrak{v} \rangle_{L^2\Lambda(\Omega)} \quad \forall \mathfrak{v} \in \mathring{\mathfrak{V}}. \tag{1.5}$$

[a] Or given the general case, we can recover $\mathfrak{p}$ by taking the mean of the n-form in $\mathfrak{f}$ and then subtract the mean to get a suitable right-hand side.

1.3 Vector Proxies

We will now state the explicit spaces we consider in 2D and 3D in terms of vector proxies, as we will need to work with them.

[1] Note that the boundary conditions are included implicitly in the domain of the operator.

1.3.1 Three Dimensions

We find that for the operator d in 3D, (see [2, Section 4.3]) in terms of vector proxies

- $H\Lambda^0(\Omega) \equiv H^1(\Omega)$,
- $H\Lambda^1(\Omega) \equiv H(\mathrm{curl})$,
- $H\Lambda^2(\Omega) \equiv H(\mathrm{div})$,
- $H\Lambda^3(\Omega) \equiv L^2(\Omega)$.

We will recall the explicit trace operator in this case for the boundary $\partial\Omega =: \Gamma$:

$$\gamma_T : \mathcal{D}(\mathrm{d}) \quad \to \quad H^{1/2}(\Gamma) \quad \times \quad H^{-1/2}(\mathrm{curl}_\Gamma) \quad \times \quad H^{-1/2}(\Gamma) \quad =: \mathscr{H}_T,$$

where

$$\gamma_T \begin{pmatrix} U_0 \\ \mathbf{U}_1 \\ \mathbf{U}_2 \\ U_3 \end{pmatrix} \quad := \quad \begin{pmatrix} U_0|_\Gamma \\ \mathbf{n} \times (\mathbf{U}_1|_\Gamma \times \mathbf{n}) \\ \mathbf{U}_2|_\Gamma \cdot \mathbf{n} \end{pmatrix}$$

where $\cdot|_\Gamma$ is understood as the usual trace operator on $H^1(\Omega)$ and $\mathbf{n}$ denotes the unit outward normal, cf. [22, Section 2]. For more details on traces, see [2, Chapter 6], [5], [8, Section 2.1, 2.2]. As with differential forms, we denote the space of functions with zero trace in $H(\bullet)$ by $\mathring{H}(\bullet)$. Note that by definition $\mathring{H}\Lambda(\Omega) \equiv \ker \gamma_T$.

The explicit problem in 3D becomes: Given $f_0 \in L^2(\Omega)$, $\mathbf{f}_1, \mathbf{f}_2 \in \left(L^2(\Omega)\right)^3, f_3 \in L^2_*(\Omega)$, seek $u_0 \in \mathring{H}^1(\Omega), \mathbf{u_1} \in \mathring{H}(\mathrm{curl}), \mathbf{u_2} \in \mathring{H}(\mathrm{div}), u_3 \in L^2_*(\Omega)$ such that

$$\begin{aligned} \int_\Omega \operatorname{grad} u_0 \cdot \mathbf{v_1} + \operatorname{curl} \mathbf{u_1} \cdot \mathbf{v_2} + \operatorname{div} \mathbf{u_2} v_3 + \mathbf{u_1} \cdot \operatorname{grad} v_0 \\ + \mathbf{u_2} \cdot \operatorname{curl} \mathbf{v_1} + u_3 \operatorname{div} \mathbf{v_2} \, \mathrm{d}\mathbf{x} = \int_\Omega v_0 f_0 + \mathbf{v}_1 \cdot \mathbf{f}_1 + \mathbf{v}_2 \cdot \mathbf{f}_2 + v_3 f_3 \, \mathrm{d}\mathbf{x} \end{aligned} \tag{1.6}$$

for all $v_0 \in \mathring{H}^1(\Omega), \mathbf{v_1} \in \mathring{H}(\mathrm{curl}), \mathbf{v_2} \in \mathring{H}(\mathrm{div}), v_3 \in L^2_*(\Omega)$.

1.3.2 Two Dimensions

In 2D, the operators of interest to us are $d^0 = \operatorname{grad}, d^1 = \operatorname{curl}$ (note that curl now maps to scalars), and the domains are $H^1 \equiv H\Lambda^0(\Omega), H(\mathrm{curl}) \equiv H\Lambda^1(\Omega), L^2 \equiv H\Lambda^2(\Omega)$ with the trace operator

$$\gamma_T : \mathcal{D}(\mathrm{d}) \quad \to \quad H^{1/2}(\Gamma) \quad \times \quad H^{-1/2}(\Gamma) \quad =: \mathscr{H}_T,$$

which is given by

$$\gamma_T \begin{pmatrix} U_0 \\ \mathbf{U}_1 \\ U_2 \end{pmatrix} \quad := \quad \begin{pmatrix} U_0|_\Gamma \\ \mathbf{n} \times \mathbf{U}_1|_\Gamma \end{pmatrix}$$

where now $\mathbf{n} \times \mathbf{U}_1|_\Gamma$ yields a scalar in 2D.
The explicit problem in 2D becomes: Given $f_0, \in L^2(\Omega), \mathbf{f}_1 \in \left(L^2(\Omega)\right)^2, f_2 \in L^2_*(\Omega)$, seek $u_0 \in \mathring{H}^1(\Omega), \mathbf{u_1} \in \mathring{H}(\mathrm{curl}), u_3 \in L^2_*(\Omega)$ such that

$$\begin{aligned} \int_\Omega \operatorname{grad} u_0 \cdot \mathbf{v_1} + \operatorname{curl} \mathbf{u_1} v_2 + \mathbf{u_1} \cdot \operatorname{grad} v_0 + u_2 \operatorname{curl} \mathbf{v_1} \, \mathrm{d}\mathbf{x} \\ = \int_\Omega v_0 f_0 + \mathbf{v}_1 \cdot \mathbf{f}_1 + v_2 f_2 \, \mathrm{d}\mathbf{x} \end{aligned} \tag{1.7}$$

for all $v_0 \in \mathring{H}^1(\Omega), \mathbf{v_1} \in \mathring{H}(\mathrm{curl}), v_2 \in L^2_*(\Omega)$.

1.3.3 Whitney Forms

Let $V_k^h \subset H\Lambda^k(\Omega)$ denote the finite element spaces of lowest order discrete differential forms on $\mathcal{T}$, known as Whitney forms, see [12, Section 4] and [27] for more details, and $V^h := \bigoplus_{k=0}^n V_k^h$, $\mathring{V}^h := \mathring{\mathfrak{V}} \cap V^h$. Note that $\mathring{V}^h$ contains only Whitney forms with zero trace on $\partial\Omega$ or zero mean in the case of n-forms. We point out that the FEEC approach to (1.5) from [19] employs $\mathring{V}^h$ for the Galerkin discretization of (1.5).

Definition 1.5
The FEEC mass matrix $\mathrm{M}_k^{\mathrm{FEEC}}$ *is the mass matrix of* $\mathring{V}_k^h$ *w.r.t. the inner product* $\langle\cdot,\cdot\rangle_{L^2\Lambda^k(\Omega)}$. *Also, we define* $\mathrm{M}^{\mathrm{FEEC}} := \operatorname{blockdiag}\left(\mathrm{M}_0^{\mathrm{FEEC}}, \ldots, \mathrm{M}_n^{\mathrm{FEEC}}\right)$, *the mass matrix of* $\mathring{V}^h$.

Chapter 2

Structured Grids

This chapter is concerned with the discretization of the problem on $\Omega = [0,1]^k$ where $k = 2$ or 3.
The discretization of (1.5) is done using lowest order FEEC on a tensor-product mesh on the unit square/cube. If not specified otherwise, h denotes the mesh-width, i.e. $1/N$ where N is the number of elements in one direction (we will only deal with meshes with an equal number of elements in each direction).

The finite element spaces elucidated in Section 1.3 are used (up to scaling):
In 3D, we use

- Vertex-based bilinear Lagrangian elements for u_0;
- Edge-based Nédélec elements (first kind) for $\mathbf{u_1}$;
- Face-based Raviart-Thomas elements for $\mathbf{u_2}$;
- Cell-centered piece-wise constants for u_3.

In 2D, we use

- Vertex-based Bilinear Lagrangian elements for u_0;
- Edge-based Nédélec elements (first kind) for $\mathbf{u_1}$;
- Cell-centered piece-wise constants for u_2.

In both cases, we will use mass lumping (using the trapezoidal rule) to compute the integrals in the Galerkin projection.

If not further specified, A_h refers to the fully assembled Galerkin matrix on a grid with the boundary DOF dropped.

2.1 Two Dimensions

2.1.1 Local Assembly

With the degrees of freedom enumerated as in Figure 2.1, the basis functions on the reference element $[0,1]^2$ are given by (see [23])

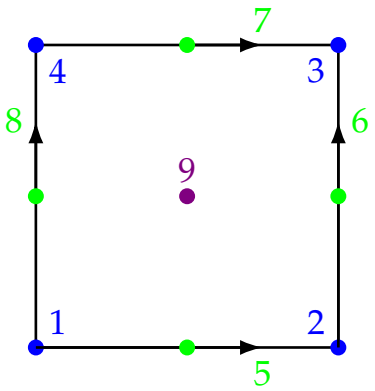

Figure 2.1: Element with the degrees of freedom as used in the 2D discretization of the problem.

- Vertex-based bilinear Lagrangian elements for u_0:

Local Index	Local Shape Function
1	$1 + xy - x - y$
2	$x(1-y)$
3	xy
4	$y(1-x)$

- Edge-centered Nédélec elements for $\mathbf{u_1}$:

Local Index	Local Shape Function
5	$\begin{pmatrix} 1-y \\ 0 \end{pmatrix}$
6	$\begin{pmatrix} 0 \\ x \end{pmatrix}$
7	$\begin{pmatrix} y \\ 0 \end{pmatrix}$
8	$\begin{pmatrix} 0 \\ 1-x \end{pmatrix}$

- Cell-centered piece-wise constants for u_3: the only DOF here is 1 with local index 9.

In order to compute the elements of the matrix, we make use of *mass lumping*, i.e. we approximate all integrals by

$$\int_{[0,1]^2} f(x)\,\mathrm{d}x \approx \frac{1}{4}\left(f(x_1) + f(x_2) + f(x_3) + f(x_4)\right),$$

where x_i are the vertices of the square.

With this enumeration of the DOF, the local element matrix (with mass lumping) of

the bilinear form on the left-hand-side of (1.7) on the reference element is

$$A_{\text{loc}} = \left[\begin{array}{cccc|cccc|c} 0 & 0 & 0 & 0 & -\frac{1}{2} & 0 & 0 & -\frac{1}{2} & 0 \\ 0 & 0 & 0 & 0 & \frac{1}{2} & -\frac{1}{2} & 0 & 0 & 0 \\ 0 & 0 & 0 & 0 & 0 & \frac{1}{2} & \frac{1}{2} & 0 & 0 \\ 0 & 0 & 0 & 0 & 0 & 0 & -\frac{1}{2} & \frac{1}{2} & 0 \\ \hline -\frac{1}{2} & \frac{1}{2} & 0 & 0 & 0 & 0 & 0 & 0 & 1 \\ 0 & -\frac{1}{2} & \frac{1}{2} & 0 & 0 & 0 & 0 & 0 & 1 \\ 0 & 0 & \frac{1}{2} & -\frac{1}{2} & 0 & 0 & 0 & 0 & -1 \\ -\frac{1}{2} & 0 & 0 & \frac{1}{2} & 0 & 0 & 0 & 0 & -1 \\ \hline 0 & 0 & 0 & 0 & 1 & 1 & -1 & -1 & 0 \end{array}\right].$$

In order to get to the element with side-length h, the integral needs to be transformed, which can be done by scaling and translating, and in the end yields an element matrix of hA_{loc}, i.e. it is just re-scaled by the mesh-width[1]. The corresponding procedure for the load vector will lead to a factor of h^2.

2.1.2 Stencil

In order to get a concrete idea of how the Galerkin matrix looks like, we explicitly compute rows corresponding to the interior DOF.

- In order to get the row corresponding to a vertex, we assemble a 2×2 grid manually, which can be seen in Figure 2.2.

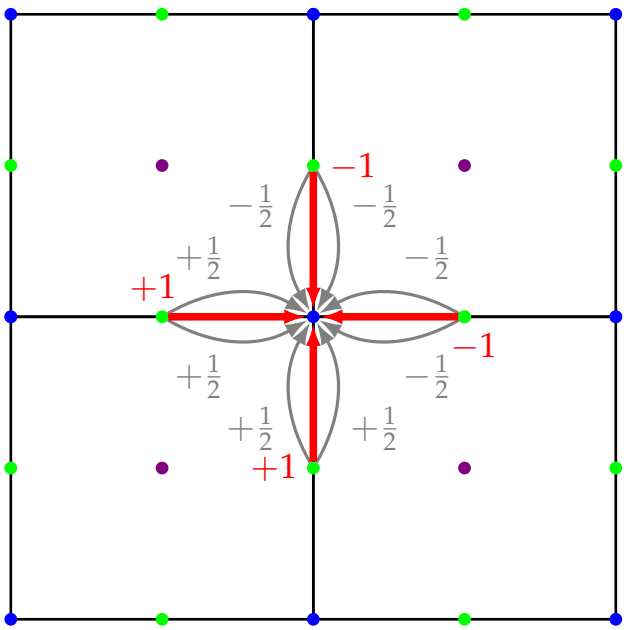

Figure 2.2: One row of the Galerkin matrix of a DOF corresponding to a vertex in units of h. The red lines indicate the coupling of the complete Galerkin matrix, whereas the grey lines indicate the contributions from the single elements.

- For an edge, we assemble a 2×1 grid (or 1×2, they yield the same, but rotated). The stencil can be found at Figure 2.3.

[1] It is not necessary to use a specific $H(\text{curl})$-conforming transformation here, as we are just re-scaling. Using it would lead to a different normalization of the basis functions, so we are technically not using the standard Whitney forns.

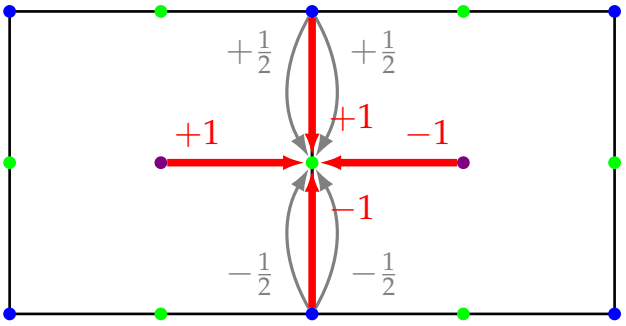

Figure 2.3: One row of the Galerkin matrix of a DOF corresponding to an edge in units of h. The red lines indicate the coupling of the complete Galerkin matrix, whereas the grey lines indicate the contributions from the single elements (for cell-centered variables the grey and red lines coincide, so the grey ones have been omitted).

- For the cell-centered variables, only one element is needed to understand all the couplings, see Figure 2.4.

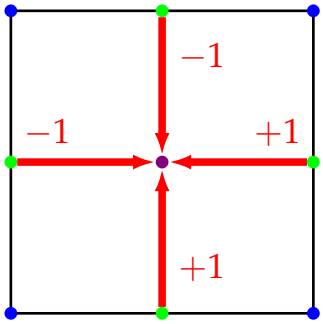

Figure 2.4: One row of the Galerkin matrix of a DOF corresponding to a cell-centered DOF in units of h. The red lines indicate the coupling of the complete Galerkin matrix.

As one can see, the matrix will be very sparse. Another convenient consequence is the fact that a matrix-free method can easily be implemented with these stencils.

To get an idea of how what the explicit matrix looks like (at least in 2D), a `python` script was written to (brute-force) assemble the matrix with the following ordering of the unknowns:

1. Vertices, left-to-right, bottom-up
2. Edges parallel to the x-axis, left-to-right, bottom-up
3. Edges parallel to the y-axis, left-to-right, bottom-up
4. Interior DOF, left-to-right, bottom-up.

The result can be seen in Figure 2.5. As is evident, A_h is populated with $\pm h$ or 0 and the diagonal vanishes.

2.1.3 Squaring the Galerkin Matrix

As can be seen in Figure 2.5, the matrix squared gives something akin to a finite-difference discretization of the (negative) Laplacian. This is a key property which can be used for the smoother, so we will now take a closer look at it. Recall that on the continuous level, "$\mathrm{D}^2 \equiv -\Delta$", which we will discover carries over in some sense to the discrete case.

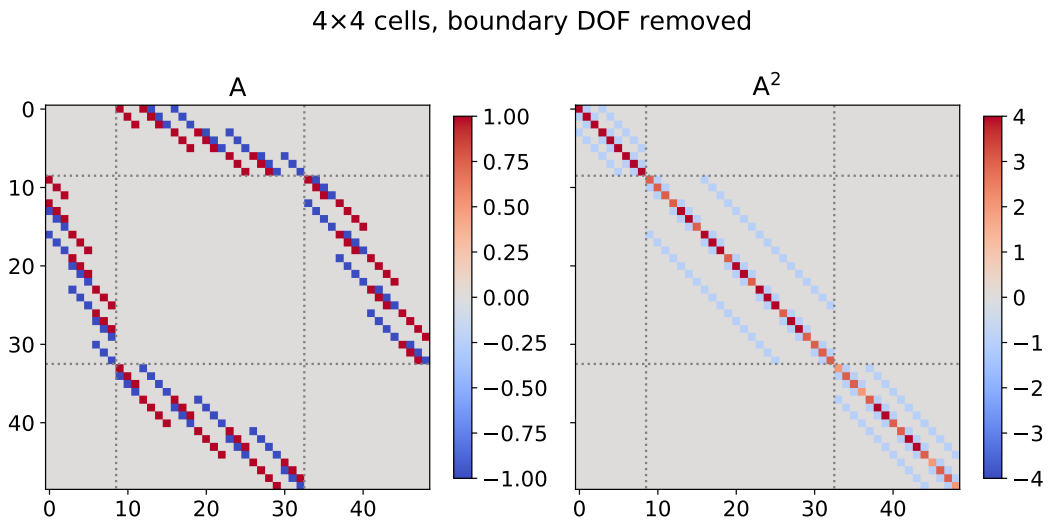

Figure 2.5: Fully assembled 2D Galerkin matrix with the boundary DOF dropped with 4×4 cells multiplied by $\frac{1}{h}$, so all entries are in units of h, and its square. The gray lines indicate the block-partitioning of the matrix corresponding to DOF associated with the nodes, edges and cells.

Remark 2.1 *Note that the property "Dirac$^2 = -\Delta$" on the discrete level is lost if we do not do mass-lumping. As an example, see Figure 2.6, where we see additional entries which couple the vertex and cell-centered DOF in the squared matrix.*

It should be mentioned that the matrix in Figure 2.6 was assembled using `MFEM` *(see [1]), hence the Galerkin matrix of the Dirac operator might differ from the one in Figure 2.5.*

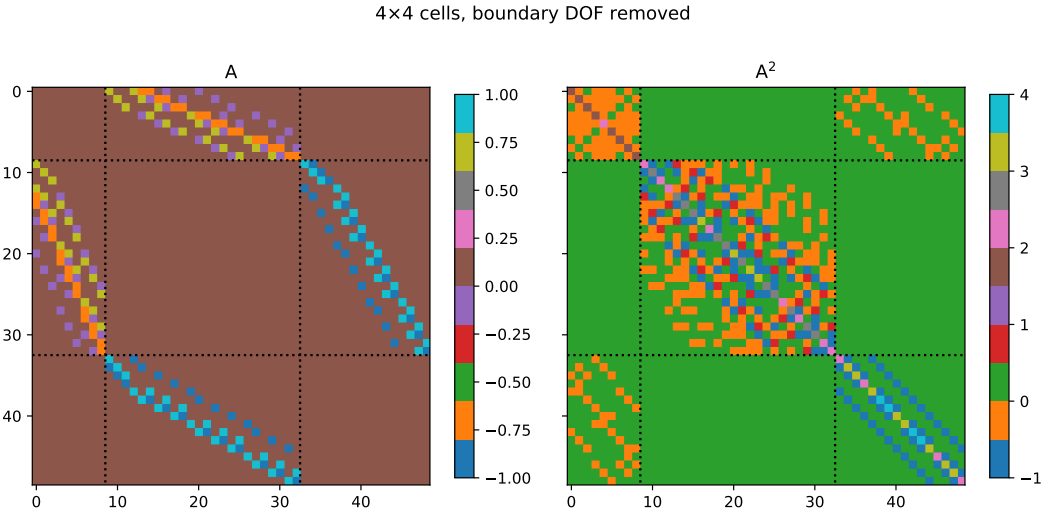

Figure 2.6: Fully assembled 2D Galerkin matrix *without mass-lumping* with the boundary DOF dropped with 4×4 cells and its square. The black lines indicate the block-partitioning of the matrix corresponding to DOF associated with the nodes, edges and cells.

It is now the time to talk abut the boundary DOF, as they will affect the squared matrix: the DOF on the boundary are dropped due to the boundary conditions from (1.7), i.e. when applying the stencil, we can just set the values accessed at the boundary to zero.

First, let us look at the 0-forms. In order to understand what happens if we apply A_h twice is to visualize it, which is done in Figure 2.7. We draw the following two conclusions:

- The violet arrows display the contribution from the cell-centered variables, which vanish due to the alternating signs;
- The blue arrows couple the vertex DOF, and we can see that the self-coupling will sum to $4h$, whereas the surrounding vertices all get an individual weight of $-1h$.

In the end, we recover the usual 5-point star for the scalar Laplacian. The boundary DOF are zero, so this will yield a block which looks like a finite-difference matrix for $-\Delta$ with Dirichlet boundary conditions. We can carry out the same procedure for one

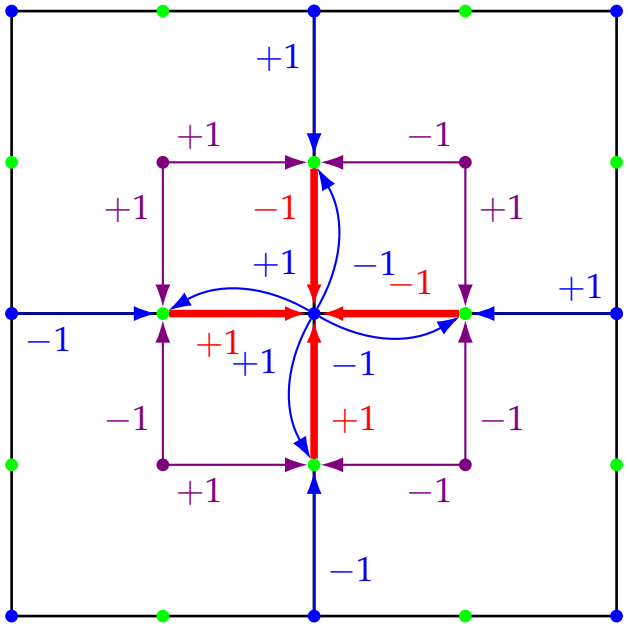

Figure 2.7: One row of the squared Galerkin matrix in 2D corresponding to a DOF on a vertex. The blue and violet arrows indicate the first application of A_h, whereas the red ones indicate the second one.

of the vector components, which will yield Figure 2.8. As before, the contributions from the other forms cancel due to alternating signs, and now also the contributions from the other vector components cancel out as well and we get a 5-star stencil for the y-component of $\mathbf{u}_1$ (i.e. the 5-point star applied to the vertical edges). Of interest is also what happens on the boundaries:

- Applying the stencil on the east and west boundaries in Figure 2.8 will yield Dirichlet boundary conditions on there, as expected.
- On the north/south boundaries, the top/bottom edge-DOF in Figure 2.8 will be missing and the edge-DOF parallel to the boundary will vanish. Hence only the contribution from the edge of interest to the vertex at the top/bottom will remain after the first application of A_h, and thus the diagonal entry of A_h^2 will be reduced by $1h$ compared to the interior, i.e. we will have $3h$ instead of $4h$. The rest remains the same.

The same considerations apply to the components on the other edges, the one parallel to the x-axis (it is the same as Figure 2.8 but rotated). One can see that this looks like

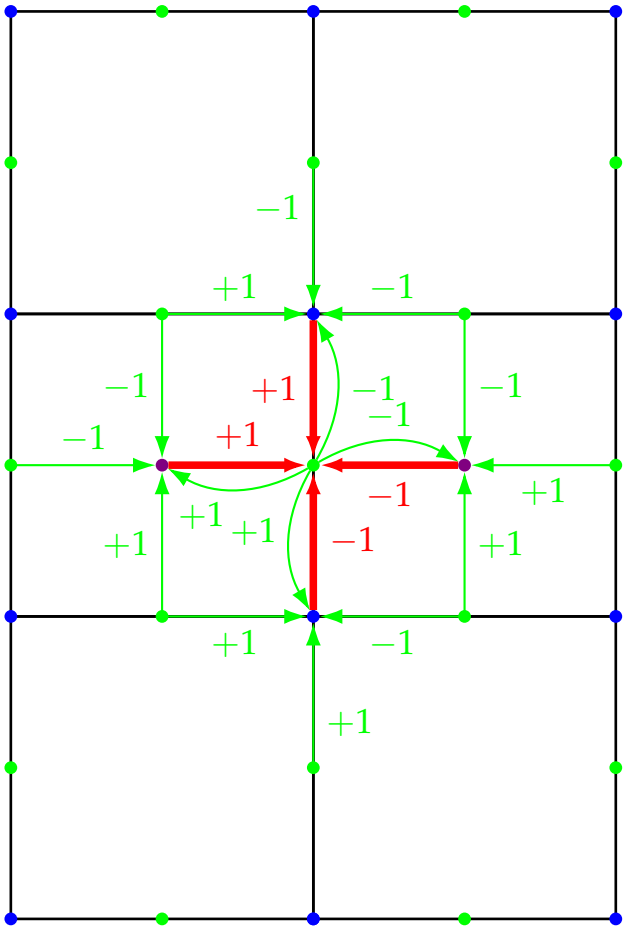

Figure 2.8: One row of the squared Galerkin matrix in 2D corresponding to a DOF on an edge. The green arrows indicate the first application of A_h, whereas the red ones indicate the second one.

a finite-difference discretization of an operator of the form

$$-\Delta \begin{pmatrix} v_1 \\ v_2 \end{pmatrix} \text{ with vanishing tangential component on } \partial\Omega.$$

Finally, the cell-centered variables will look like a discretization (up to a factor) of $-\Delta$ with Neumann boundary conditions

$$-\Delta v \text{ with } \boldsymbol{\nabla} v \cdot \mathbf{n} = 0 \text{ on } \partial\Omega,$$

i.e. the 5-point star is applied with ghost cells which hold the value of the nearest cell at the boundary. The figure is omitted for the sake of brevity.

This will lead to a reduction of the diagonal entry by the number of adjacent "ghost cells" when compared to the interior, i.e. the diagonal entry will be $4h$ in the interior, $3h$ if the cell neighbors exactly one boundary, and $2h$ if it is in a corner.

Zooming into A_h^2 in Figure 2.5 yields Figure 2.9, and we can see that indeed the diagonal entries vary as expected (see the previous section for the enumeration of the DOF).

2.2 Three Dimensions

Here, there are 27 DOF on the reference element. The enumeration of the local shape functions can be found in Figure 2.10. The explicit expressions of the local

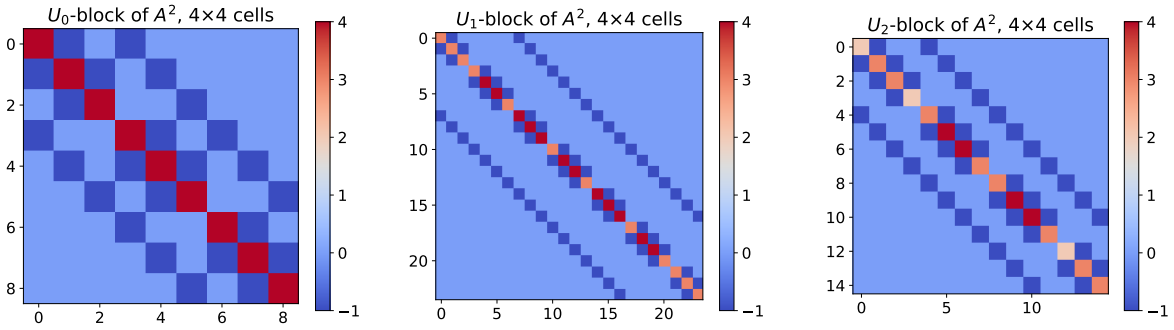

Figure 2.9: Zoom-in of A_h^2 from Figure 2.5.

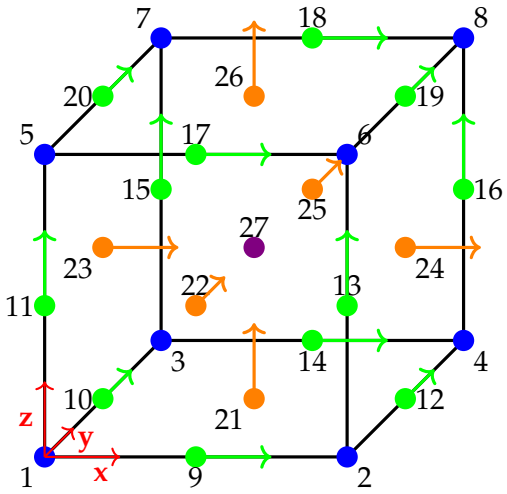

Figure 2.10: Enumeration of the DOF on the cube.

shape functions can be found in Appendix A. Here, the computation of the local element matrix yields a 27×27 matrix, which is quite unwieldy, so `sympy` was used to carry out the local calculations symbolically, the result of which can also be found in Appendix A. It is easy to check that the element matrix now scales with h^2 instead of h like in the 2D case. The entries in load vector now also scale with h^3 instead of h^2.

Explicitly looking at the entries of the element matrix, we observe the following:

- DOF associated with the vertices only have entries $\pm\frac{1}{4}$,
- DOF associated with the edges only have entries $\pm\frac{1}{4}$,
- DOF associated with the faces only have entries $\pm\frac{1}{2}$, and
- DOF associated with the cell-center only have entries ± 1

in their respective rows/columns in the element matrix. For the edges and faces, it is exactly ± 1 the reciprocal of the number of DOF which are shared by the cubes in the interior of the grid. So like in the 2D case, assembling the matrix will then lead to entries of only ± 1 (in units of h^2). To see this, let us look at a $2 \times 2 \times 2$ grid and assemble the row corresponding to a DOF on the middle vertex, as in Figure 2.11. As can be seen, the entries sum to ± 1, and this fact carries over to the other DOF as well, but the explicit computation is omitted for the sake of brevity.

The square of the matrix can be computed by the same means as in the 2D case, except

that now the stencils contain more elements and it is harder to visualize. For concrete numbers, see Appendix A. In the end, we find that (in units of h^2)

- For u_0, we get the 7-point stencil with Dirichlet boundary conditions, the diagonal is constant $\equiv 6$;
- For $\mathbf{u}_1$, we get the 7-point stencil with boundary condition $\mathbf{u}_1|_{\partial\Omega} \times \mathbf{n} = 0$, the diagonal is constant $\equiv 6$ on the interior, and at points on the boundary 5;
- For $\mathbf{u}_2$, we get the 7-point stencil with boundary condition $\mathbf{u}_2|_{\partial\Omega} \cdot \mathbf{n} = 0$, the diagonal is constant $\equiv 6$ on the interior, at points on exactly one boundary 5, and on exactly two boundaries 4;
- For u_3, we get the 7-point stencil with (like in 2D) mirrored ghost cells, the diagonal is constant $\equiv 6$ on the interior, at cells on exactly one boundary 5, on exactly 2 boundaries 4, and 3 at the corner cells of the cube.

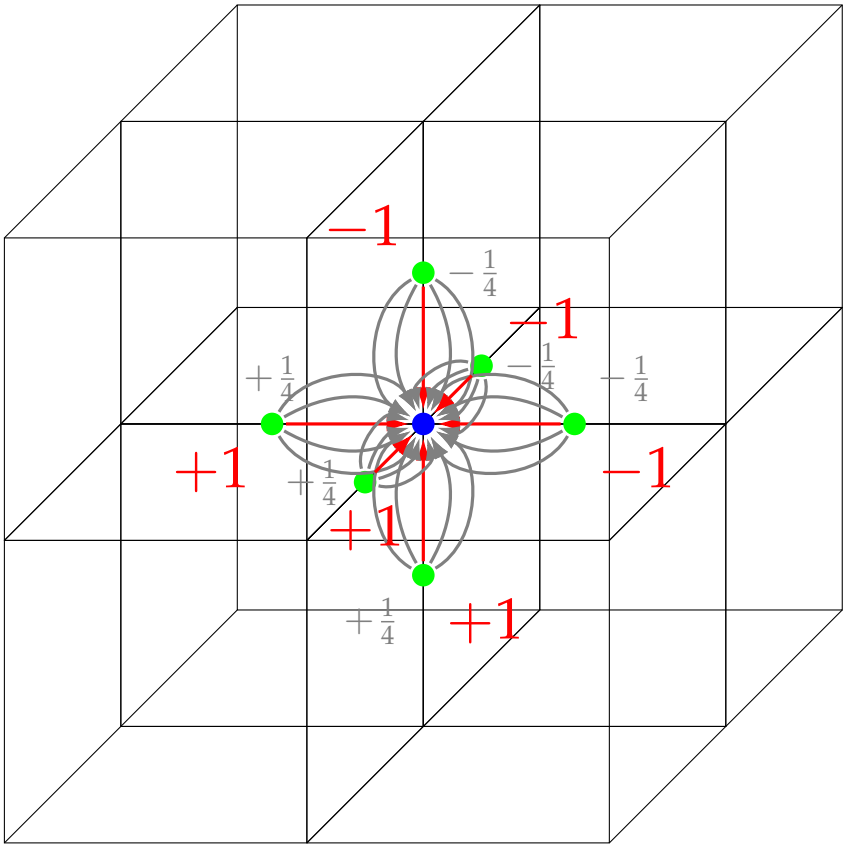

Figure 2.11: One row of the 3D Galerkin matrix of a DOF corresponding to a vertex in units of h^2. The gray arrows indicate the contributions from the single elements, whereas the red ones indicate the entries in the assembled matrix.

2.3 Zero Mean Condition

The linear system to solve in the end has the form

$$A_h u_h = f_h. \tag{2.1}$$

The DOF on the boundary are dropped due to the boundary conditions from (1.7) or (1.6). However, we still need to augment the system to make sure that the second scalar component is in $L^2_*(\Omega)$, see (1.7) and (1.6).

Without these zero-mean conditions, we expect A_h to be singular. Specifically, as this is a mean-zero condition for the second scalar component, the matrix will have a one-dimensional kernel

$$\ker A_h = \operatorname{span}\left\{(0,\dots,0,1,\dots,1)^T\right\},$$

i.e. constant n-forms, where n is the dimension. The extended system is thus equivalent to seeking a solution to (2.1) in $(\ker A_h)^\perp$.

Note that $\operatorname{ran} A_h = \left(\ker A_h^T\right)^\perp = (\ker A_h)^\perp$, as $A_h = A_h^T$. This also implies that the part of f_h corresponding to the n-forms must have mean zero for a solution to exist, as $f_h \in \operatorname{ran} A_h$ has to be fulfilled. If quadrature is used to compute the load vector, this condition can be violated, so we have to be careful. A potential option is to subtract the mean of the second scalar component, which can incur a source of error in the load vector.

See [13, Chapter 12.1.2] for a discussion on this (i.e. singular) and related problems.

2.4 Distributive Relaxation

2.4.1 Transforming Smoothers

Since the Galerkin matrices have zeros on the diagonal, a simple smoother like Gauss-Seidel or Jacobi cannot be applied directly. Instead, the idea with transforming smoothers is to transform the system into one where we can apply a known smoothing procedure, and then transform back accordingly, see [26] for a more rigorous description of this topic. In the notation of [26], given some matrix K for which we want a smoother, we define a matrix-splitting via a transformation with (invertible) matrices $\bar{K}$ and $\bar{\bar{K}}$, called r- and l-transformations respectively, by

$$\tilde{K} := \bar{\bar{K}} K \bar{K} = M - N,$$

where $M - N$ is a suitable splitting, e.g. $M = \operatorname{tril}(\tilde{K})$ for Gauss-Seidel.

> **Remark 2.2 (Intuition/Motivation)** *If we know that we can find a good approximate inverse $M^{-1} \approx \tilde{K}^{-1}$, we can translate that into one for K via*
>
> $$\bar{K}\tilde{K}^{-1}\bar{\bar{K}} = \bar{K}\left(\bar{\bar{K}} K \bar{K}\right)^{-1}\bar{\bar{K}} = K^{-1},$$
>
> *so using $\bar{K}M^{-1}\bar{\bar{K}}$ as the matrix for the smoother seems sensible. Note that the inverse of $\bar{K}, \bar{\bar{K}}$ is never needed in explicit form.*

A step in the smoother for a given right-hand-side f is then defined by

$$u \mapsto u + \bar{K}M^{-1}\bar{\bar{K}}\left(f - Ku\right).$$

2.4.2 DGSR and Convergence

Given A_h from (2.1), we know that A_h^2 has the structure of the finite-difference matrix of $-\Delta$ with suitable boundary conditions. More importantly,

$$A_h^2 = (L + D) + U,$$

where L is the lower triangular, $U = L^T$ the upper triangular part and D the diagonal of A_h^2, for which $D > 0$ holds. Therefore, $M_{\mathrm{GS}} := L + D$ is invertible.

The method proposed is a kind of r-transforming (r-transforming meaning $\bar{\bar{K}} = I$) smoother with $\bar{K} = A_h$:

$$u_h^{i+1} = u_h^i + \underbrace{A_h M_{\text{GS}}^{-1} \left(f_h - A_h u_h^i \right)}_{\in \operatorname{ran} A_h}. \tag{2.2}$$

Notice that if $u_h^k \in \operatorname{ran} A_h = (\ker A_h)^\perp$, then $u_h^{k+1} \in \operatorname{ran} A_h$. This means that if the method converges with an initial vector in $(\ker A_h)^\perp$, it converges to the desired solution with mean zero and the system need not be extended, cf. Section 2.3.

Remark 2.3 *We could also use the corresponding l-transforming smoother (meaning $\bar{K} = I$), i.e.*

$$u_h^{i+1} = u_h^i + M_{\text{GS}}^{-1} A_h \left(f_h - A_h u_h^i \right).$$

This is the smoother we get if we tackle the squared system

$$A_h u = f \implies A_h^2 u = A_h f$$

with Gauss-Seidel. As A_h^2 is the matrix of the Laplacian discretized with finite-differences, we can solve it using standard multigrid methods, now with the right-hand-side $A_h f$.

Let now $u_h^* \in (\ker A_h)^\perp$ be the unique solution to $A_h u_h^* = f_h$. Then the error at iteration $k+1$ is given by

$$u_h^{k+1} - u_h^* = \underbrace{\left(1 - A_h M_{\text{GS}}^{-1} A_h \right)}_{=:E} (u_h^k - u_h^*).$$

In the spirit of [24, Chapter 12.3], we can prove the following.

Proposition 2.4

$$\forall x \in (\ker A_h)^\perp \setminus \{0\} : \|Ex\| < \|x\|.$$

Proof Let $\langle \cdot, \cdot \rangle$ denote the standard inner product on vectors.
We get

$$\begin{aligned}
\langle Ex, Ex \rangle &= \langle x, x \rangle - \left\langle x, A_h M_{\text{GS}}^{-1} A_h x \right\rangle - \left\langle A_h M_{\text{GS}}^{-1} A_h x, x \right\rangle + \left\langle A_h M_{\text{GS}}^{-1} A_h x, A_h M_{\text{GS}}^{-1} A_h x \right\rangle \\
&= \langle x, x \rangle - \left\langle A_h x, M_{\text{GS}}^{-1} A_h x \right\rangle - \left\langle M_{\text{GS}}^{-1} A_h x, A_h x \right\rangle + \left\langle A_h M_{\text{GS}}^{-1} A_h x, A_h M_{\text{GS}}^{-1} A_h x \right\rangle,
\end{aligned}$$

as A_h is self-adjoint.

Now make the substitution $z := M_{\text{GS}}^{-1} A_h x \iff M_{\text{GS}} z = A_h x$. Then:

$$\begin{aligned}
\langle Ex, Ex \rangle &= \langle x, x \rangle - \left\langle x, A_h M_{\text{GS}}^{-1} A_h x \right\rangle - \left\langle A_h M_{\text{GS}}^{-1} A_h x, x \right\rangle + \left\langle A_h M_{\text{GS}}^{-1} A_h x, A_h M_{\text{GS}}^{-1} A_h x \right\rangle \\
&= \langle x, x \rangle - \left\langle A_h x, M_{\text{GS}}^{-1} A_h x \right\rangle - \left\langle M_{\text{GS}}^{-1} A_h x, A_h x \right\rangle + \left\langle A_h M_{\text{GS}}^{-1} A_h x, A_h M_{\text{GS}}^{-1} A_h x \right\rangle \\
&= \langle x, x \rangle - \langle M_{\text{GS}} z, z \rangle - \langle z, M_{\text{GS}} z \rangle + \langle A_h z, A_h z \rangle.
\end{aligned}$$

What is left to prove is

$$\langle A_h z, A_h z \rangle < \langle M_{\text{GS}} z, z \rangle + \langle z, M_{\text{GS}} z \rangle = \left\langle \left(M_{\text{GS}} + M_{\text{GS}}^T \right) z, z \right\rangle.$$

We have

$$\begin{aligned}\left\langle \left(M_{\mathrm{GS}} + M_{\mathrm{GS}}^T\right) z, z \right\rangle &= \left\langle \left((D+L) + \left(D + L^T\right)\right) z, z \right\rangle \\ &= \left\langle \left(A_h^2 + D\right) z, z \right\rangle \\ &= \langle A_h z, A_h z \rangle + \langle Dz, z \rangle \\ &> \langle A_h z, A_h z \rangle ,\end{aligned}$$

as we know that $D > 0$ and that $z \neq 0$ by the assumption of the lemma: $0 \neq x \in (\ker A_h)^\perp \implies z = M_{\mathrm{GS}}^{-1} A_h x \neq 0$. □

Remark 2.5 *Strictly speaking convergence of the smoother is not a necessary assumption, yet it is still good to know for testing purposes. The following is not supposed to be a rigorous proof, but a motivation as for why we may expect the smoother to perform well.*

In [26, Theorem 2.2.1] it is proven that (for invertible matrices) we need the smoothening property (from [13, Chapter 6]) of the product system, i.e. Gauss-Seidel for A_h^2 in our case, in order to conclude two-grid convergence.

More precisely, for a sequence of meshes indexed by l, in [26, Theorem 2.2.1] it is presumed that there exist $\eta(\nu), \nu'(h)$ such that

$$\eta(\nu) \to 0 \quad \text{for } \nu \to \infty, \qquad \nu'(h) = \infty \quad \text{or} \quad \nu'(h) \to \infty \quad \text{for } h \to 0$$

and

$$\|K_l \bar{K}_l S_l^\nu\| \leq C\eta(\nu) \quad \text{for } 0 < \nu < \nu'(h_l),\ l \geq 2,$$

where $K_l, \bar{K}_l$ denote the Galerkin matrix and the respective r-transformation on the l-th refinement level, S_l^ν refers to the ν-times applied smoother at level l and $\|\cdot\|$ refers to a suitable norm, see [26] for more details.

Other assumptions regarding the stability and the "approximation property" (see again [26], [13, Chapter 6]) enter in the theorem statement, which we assume to be fulfilled as we are working with standard finite-differences/finite-elements.

In our case, we have $K_l = \bar{K}_l = A_h$ and the smoothing property above boils down to the one from [13, Chapter 6] for Gauss-Seidel applied to A_h^2, the standard finite-difference discretization of the Laplacian. Hence, we may anticipate a well-behaved method as Gauss-Seidel (as a smoother) is expected to perform well on the finite-difference Laplacian.

In practice (2.2) can be made more efficient. [13, Chapter 11.3] describes in-place operations, which is interesting especially in 3D, as the memory requirements are quite demanding.

It works by "distributing" the update after each step, i.e. for each $i = 1, \ldots, N_{\mathrm{dof}}$, where N_{dof} is the number of degrees of freedom (assume some ordering of the DOF), do the following:

1. Find the correction Δu_h^i for the Gauss-Seidel step with A_h^2 for the i-th component

$$(\Delta u_h^i)_j := \frac{\delta_{ij}}{D_{ii}} \left(f_h - A_h u_h\right)_i ,$$

   where δ_{ij} is the Kronecker delta.

2. Distribute the correction

$$u_h \leftarrow u_h + A_h \Delta u_h^i.$$

The advantage is that this can be done in-place if we know what A_h does to a single DOF, which is trivial for structured grids as we know the stencils.

2.4.3 A Simple Parallelization Strategy on Structured Grids

The disadvantage of the above approach is that it cannot be parallelized at all: the update of the next component depends on the values of previous one. There are methods one could employ to ameliorate the issue, as mentioned in [18], however this is not the topic of this thesis, so a simple approach will be take to at least gain some speedup, as the 3D problems become quite large.

In order to parallelize DGSR, we can divide the DOF into subsets which do not interfere with one another ("red-black splitting", see [18]), and apply Gauss-Seidel in parallel to each of the blocks of unknowns.

In our problem the stencils are local, so splitting the DOF into odd and even indices in the outer loop and parallelizing the outer loop appears sensible.

To see how this works, let us look at an explicit example for the 3D 0-forms. The serial loop for that part is listed in Figure 2.12. As can be seen the outer loop is over z, so

```
for(unsigned int kz = 1; kz < N; ++kz) {
    for(unsigned int ky = 1; ky < N; ++ky) {
        for(unsigned int kx = 1; kx < N; ++kx) {
          const SCALAR diag_element = 6 * h * h;
          // The value to distribute
          const SCALAR val =
            (
             rhs.U0(kx, ky, kz) -
             h * h *
             (
               U10(kx - 1, ky, kz) +
               U11(kx, ky - 1, kz) +
               U12(kx, ky, kz - 1) -
               U10(kx, ky, kz) -
               U11(kx, ky, kz) -
               U12(kx, ky, kz)
             )
            ) / diag_element;
          // Distribute
          U10(kx - 1, ky, kz) += val;
          U11(kx, ky - 1, kz) += val;
          U12(kx, ky, kz - 1) += val;
          U10(kx, ky, kz)     -= val;
          U11(kx, ky, kz)     -= val;
          U12(kx, ky, kz)     -= val;
        }
    }
}
```

Figure 2.12: Serial code for one DGS step for the 0-form in the 3D case. `U1i` denotes the i-th component of (the approximation of) $\mathbf{u}_1$.

we proceed to split the loop into two by iterating separately over a loop starting at $k_z = 0$ in steps of $k_z \leftarrow k_z + 2$, and another one with $k_z = 1$ with the same step size. Every loop now iterates over "slabs" in z, and the elements inside the loops which are accessed and modified are not shared by any two threads if only the *outer loop* is parallelized, as only entries in k_z and $k_z - 1$ are accessed and modified.

[18] explains more ways in which one could further optimize this, e.g. by using

blocking to better utilize cache and doing several iterations with each block, but this is outside the scope of this thesis.

2.5 Numerical Results

2.5.1 Two Dimensions

Unit Square

In order to test whether the convergence of the multigrid method is sound, a power iteration was used to determine the convergence rate of one V-cycle, which can be found in Table 2.1. We observe mesh-width independent convergence rates, which is

N	$\lvert\lambda_{\max}\rvert$
16	0.127139
32	0.155516
64	0.180073
128	0.179090
256	0.179597
512	0.180109
1024	0.180379
2048	0.180386
4096	0.180453
8192	0.180490

Table 2.1: Estimated multigrid convergence rates in 2D with $N \times N$ cells. The coarse solver was used at $N = 8$.

what is desired from a multigrid method.

To ensure that the solver is computing the correct solution, a solution was manufactured. A solution to (1.7) is

$$u_0 = \sin 2\pi x \sin 2\pi y, \quad \mathbf{u}_1 = (\sin 2\pi y, \sin 2\pi x)^T, \quad u_2 = \cos 2\pi x \sin 2\pi y$$

with a suitable right-hand-side. Midpoint quadrature was used to assemble the load vector. Coincidentally, since the sine and cosine exhibit a lot of symmetry, this leads to a load vector where the zero mean condition is already fulfilled. From Table 2.2, we see that the method converges towards the correct solution (in L^2).

L-domain

The domain was changed to $[0,1]^2 \setminus \left[\frac{1}{2},1\right]^2$, and the same experiments were performed by "ignoring" the unknowns on $\left[\frac{1}{2},1\right]^2$ in the previous code.

The multigrid method converges independently of the mesh-width, albeit more slowly than on the unit square, as can be seen in Table 2.3.

2.5.2 Three Dimensions

Similar to 2D, we used a unit cube $[0,1]^3$ to test the solver, the convergence rates of which for a V-cycle were estimated using a power iteration, see Table 2.4 for the results. The convergence rates appear to be independent of the mesh-width.

N	L^2-Error	EOC
8	3.205e-02	-
16	7.892e-03	2.022e+00
32	1.963e-03	2.007e+00
64	4.901e-04	2.002e+00
128	1.225e-04	2.000e+00
256	3.062e-05	2.000e+00
512	7.658e-06	2.000e+00
1024	1.921e-06	1.995e+00
2048	4.802e-07	2.000e+00
4096	1.200e-07	2.000e+00
8192	3.001e-08	2.000e+00

Table 2.2: L^2-convergence of the 2D method on the unit square.

N	$\lvert\lambda_{\max}\rvert$
16	0.127750
32	0.205109
64	0.256203
128	0.277636
256	0.295125
512	0.313239
1024	0.330512
2048	0.317173
4096	0.347785
8192	0.354167

Table 2.3: Estimated multigrid convergence rates in 2D on the L-domain with $N \times N$ cells. The coarse solver was used at $N = 8$.

N	$\lvert\lambda_{\max}\rvert$
16	0.192022
32	0.254523
64	0.268223
128	0.277890
256	0.277934
512	0.278920

Table 2.4: Estimated multigrid convergence rates in 3D with $N \times N \times N$ cells. The coarse solver was used at $N = 8$.

To verify that the solver is solving the correct equation, a solution was again manufactured. This time, the manufactured problem is given by

$$
\begin{aligned}
u_0 &= \sin(2x\pi)\sin(2y\pi)\sin(2z\pi),\\
u_1 &= (\sin(2y\pi)\sin(2z\pi)\cos(2x\pi))\,\hat{i} + (\sin(2x\pi)\sin(2z\pi)\cos(2y\pi))\,\hat{j}\\
&\quad + (\sin(2x\pi)\sin(2y\pi)\cos(2z\pi))\,\hat{k},\\
u_2 &= (\sin(2x\pi)\cos(2y\pi)\cos(2z\pi))\,\hat{i} + (\sin(2y\pi)\cos(2x\pi)\cos(2z\pi))\,\hat{j}\\
&\quad + (\sin(2z\pi)\cos(2x\pi)\cos(2y\pi))\,\hat{k},\\
u_3 &= \cos(2x\pi)\cos(2y\pi)\cos(2z\pi)
\end{aligned}
$$

and an appropriate right-hand-side, where $\hat{i}, \hat{j}, \hat{k}$ denote the unit vectors in the corresponding directions. As in 2D, midpoint quadrature was used to assemble the load vector, and as before, the mean is already zero. From Table 2.5, we see that the

N	L^2-Error	EOC
16	6.401e-03	-
32	1.581e-03	2.017e+00
64	3.944e-04	2.003e+00
128	9.864e-05	1.999e+00
256	2.467e-05	1.999e+00
512	6.117e-06	2.012e+00

Table 2.5: L^2-convergence of the 3D method.

solution converges towards the correct solution (in L^2).

In Table 2.5 we can only go up to 512^3 cells, as the memory requirements become quite steep, even when using single precision. In contrast, in the 2D case in Table 2.2, we can easily go up to 8192^2 cells with double precision and without any explicit parallelization.

Chapter 3

Unstructured Grids

3.1 Motivation: Dual Grid Perspective

Let us analyze in detail what exactly happens if we square the Galerkin matrix in 2D on a more abstract level on a *structured grid*. This section is meant to motivate the approach with discrete exterior calculus.

Let $\mathring{V}_k^h$ be spaces like in Section 1.3.3, in our case $\mathring{V}_0^h \equiv$ nodal elements, $\mathring{V}_1^h \equiv$ Nédélec elements and $\mathring{V}_2^h \equiv$ piece-wise constants, and let $D_k := \mathrm{d}|_{\mathring{V}_k^h}$ be the (matrix of the) exterior derivative on these spaces (recall: $\mathrm{d}_0 \equiv \nabla$ and $\mathrm{d}_1 \equiv \vec{\nabla}\times$).

Then for $\omega_k \in V_k^h, \nu_{k-1} \in V_{k-1}^h$, we have

$$\langle \omega_k, \mathrm{d}\nu_{k-1} \rangle_{L^2\Lambda^k(\Omega)} = \vec{\omega}_k^T \mathrm{M}_k^{\mathrm{FEEC}} D_{k-1} \vec{\nu}_{k-1}, \tag{3.1}$$

where $\vec{\bullet}$ denotes the corresponding coefficient vector. Using this (and the transpose thereof), we conclude that the Galerkin matrix is given by

$$A_h = \begin{pmatrix} 0 & D_0^T \mathrm{M}_1^{\mathrm{FEEC}} & 0 \\ \mathrm{M}_1^{\mathrm{FEEC}} D_0 & 0 & D_1^T \mathrm{M}_2^{\mathrm{FEEC}} \\ 0 & \mathrm{M}_2^{\mathrm{FEEC}} D_1 & 0 \end{pmatrix}$$

$$\implies A_h^2 = \begin{pmatrix} D_0^T \mathrm{M}_1^{\mathrm{FEEC}} \mathrm{M}_1^{\mathrm{FEEC}} D_0 & 0 & D_0^T \mathrm{M}_1^{\mathrm{FEEC}} D_1^T \mathrm{M}_2^{\mathrm{FEEC}} \\ 0 & D_1^T \mathrm{M}_2^{\mathrm{FEEC}} \mathrm{M}_2^{\mathrm{FEEC}} D_1 + \mathrm{M}_1^{\mathrm{FEEC}} D_0 D_0^T \mathrm{M}_1^{\mathrm{FEEC}} & 0 \\ \mathrm{M}_2^{\mathrm{FEEC}} D_1 \mathrm{M}_1^{\mathrm{FEEC}} D_0 & 0 & \mathrm{M}_2^{\mathrm{FEEC}} D_1 D_1^T \mathrm{M}_2^{\mathrm{FEEC}} \end{pmatrix}.$$

In the case of structured grids, the *mass-lumped* mass matrices become multiples of the identity and since $D_1 D_0 = 0$, the off-diagonal terms cancel. In the unstructured case, or even just the structured case without mass lumping, this will not happen and we can see that "$A_h^2 = -\Delta$" will fail in general.

Furthermore, we know that (with mass lumping) $\mathrm{M}_2^{\mathrm{FEEC}} D_1 D_1^T \mathrm{M}_2^{\mathrm{FEEC}}$ yields finite-differences on cell-centered variables. This is curious, as it does not make much sense to use cell-centered piece-wise constant finite elements to discretize the Laplacian. Or rather, it is a mass-lumped nodal finite element discretization of the Laplacian on a grid connecting the cell-centers, a *dual grid*.

The notion of a dual grid in the structured case in 2D is clear as one can identify the mesh entities on the primal and dual grid. Explicitly, we can identify

- Nodes on the primal grid with cell-centers on the dual grid;

- Edges on the primal grid with edges on the dual grid;
- Cell-centers on the primal grid with nodes on the dual grid.

To see how things clear up in this perspective, define an operator s_k mapping from the finite-element space on the primal mesh to the one on the dual mesh via

$$s_k \vec{\omega}_k := \mathrm{M}_k^{\mathrm{FEEC}} \vec{\omega}_k,$$

where $\vec{\omega}_k$ denotes the coefficients of a finite-element function ω_k. It takes nodes to cell-centers and edges to edges, which works as the boundary DOF are dropped (recall: we are assuming essential boundary conditions), so the number of primal nodes equals the number of dual cells. In the end, we get

$$\left(\mathrm{M}^{\mathrm{FEEC}}\right)^{-1} A_h = \begin{pmatrix} 0 & s_0^{-1} D_0^T s_1 & 0 \\ D_0 & 0 & s_1^{-1} D_1^T s_2 \\ 0 & D_1 & 0 \end{pmatrix}, \tag{3.2}$$

where we recall that $\mathrm{M}^{\mathrm{FEEC}} = \mathrm{blockdiag}\left(\mathrm{M}_0^{\mathrm{FEEC}}, \mathrm{M}_1^{\mathrm{FEEC}}, \mathrm{M}_2^{\mathrm{FEEC}}\right)$. In this form, the blocks are reminiscent of concepts from exterior calculus: s_k is related to the *Hodge-Star* and $s_k^{-1} D_k^T s_{k+1}$ to the *codifferential*.

3.2 Discrete Exterior Calculus

3.2.1 Cellular Complexes

We briefly introduce some notation regarding cellular complexes, but a complete description will not be given, as it is not the main topic of this thesis. For more details refer to [15, Chapter 3], [7, Section 5.1], [6, Section 3].

Let $\mathcal{T}$ be an oriented simplicial mesh of $\Omega \subset \mathbb{R}^n$ and write $\mathcal{T}^k$ for the k-cells of $\mathcal{T}$ and $C^k(\mathcal{T})$ the k-cochains on $\mathcal{T}$, see [7, around p. 69] for more details.

Furthermore, let the coboundary operator be denoted by $\partial^k : C^k(\mathcal{T}) \to C^{k+1}(\mathcal{T})$. The matrix of ∂^k w.r.t. the standard basis of $C^k(\mathcal{T})$ is the *incidence matrix* between (oriented and active) k- and $(k+1)$-dimensional cells. It can be shown (see [7, Lemma 5.4]) that $\partial^{k+1}\partial^k \equiv 0$.

Let $\langle \mathsf{u}, \sigma \rangle \equiv \mathsf{u}(\sigma)$ denote the duality pairing of $\mathsf{u} \in C^k(\mathcal{T})$ and $\sigma \in \mathcal{T}^k$.

Remark 3.1 *Notice how in the structured case in Figure 2.5 the matrix only has entries in $\{-1, 0, 1\}$ (in units of h). This is related to the* coboundary *operator, which when understood as the matrix of a linear map, only contains entries in $\{-1, 0, 1\}$.*

Definition 3.2 ([7, p. 72])
The de Rham map, denoted by $\mathcal{R}^k : \Lambda^k(\Omega) \to C^k(\mathcal{T})$ is defined by $\mathcal{R}^k \omega = \mathsf{w}$, where

$$\langle \mathsf{w}, \sigma \rangle = \int_\sigma \omega \quad \forall \sigma \in \mathcal{T}^k.$$

We define the de Rham map on $\Lambda(\Omega)$ by $\mathcal{R} := \bigoplus_k \mathcal{R}^k$.

Definition 3.3 (Whitney Map)
The Whitney map on k-cochains is the isomorphism onto Whitney k-forms $\mathcal{W}^k : C^k(\mathcal{T}) \to V_h^k$*, given by* $\mathcal{W}^k w = \sum_{\sigma \in \mathcal{T}^k} \varphi_\sigma \langle w, \sigma \rangle$ *where* $w \in C^k(\mathcal{T})$ *and* φ_σ *is the Whitney form associated to* σ*. Also, let* $\mathcal{W} := \bigoplus_{k=0}^{n} \mathcal{W}^k$*.*

Note that $\mathcal{W}^k$ is represented by an identity matrix with respect to the standard bases of $C^k(\mathcal{T})$ and V_k^h.

Definition 3.4
Define $\mathring{C}(\mathcal{T}) := \bigoplus_{k=0}^{n-1} \mathring{C}^k(\mathcal{T}) \oplus C_*^n(\mathcal{T})$*, where* $\mathring{C}^k(\mathcal{T})$ *are k-cochains with zero values on the boundary and* $C_*^n(\mathcal{T})$ *is the space of n-cochains with vanishing mean, i.e.* $\mathsf{w} \in C_*^n(\mathcal{T}) \implies \sum_{\sigma \in \mathcal{T}^n} \langle \mathsf{w}, \sigma \rangle = 0$*.*

3.2.2 Hodge Stars and Dual Grids

Definition 3.5 (Dual Mesh, [14, Definition 3])
Two meshes $\tilde{\mathcal{T}}$ *and* $\mathcal{T}$ *covering an n-dimensional manifold are called (topologically) dual to each other if* $L_l^T = (-1)^{l+1} \tilde{L}_{n-(l+1)}, 0 \leq l < n$*, where* L_l *and* $\tilde{L}_l$ *are the incidence matrices of oriented l- and* $(l+1)$*-facets of* $\mathcal{T}$ *and* $\tilde{\mathcal{T}}$*, respectively.*

The above implies that being dual also means that there is a one-to-one correspondence between the k-cells on the primal and $(n-k)$-cells on the dual mesh.

Denote the identification map between the primal and dual mesh cells by

$$*_k : \mathcal{T}^k \to \tilde{\mathcal{T}}^{n-k}.$$

For more on this, see [14, Section 5] and [12, Definition 3.3].

Henceforth we will assume that none of the cells in either the primal or dual mesh are degenerate, i.e. have zero volume.

Definition 3.6 (Discrete Hodge Star, [12, Definition 3.6])
Let $|\sigma|$ *denote the volume of a cell* $\sigma \in \mathcal{T}$*. The discrete Hodge star on cochains is the operator* $\bigstar_k : C^k(\mathcal{T}) \to C^{n-k}(\tilde{\mathcal{T}})$ *such that for* $\mathsf{w} \in C^k(\mathcal{T})$

$$\frac{1}{|*\sigma|} \langle \bigstar_k \mathsf{w}, *\sigma \rangle = \frac{1}{|\sigma|} \langle \mathsf{w}, \sigma \rangle \quad \forall \sigma \in \mathcal{T}^k.$$

We define $\bigstar_k^{-1}$ *by*

$$\frac{1}{|\sigma|} \left\langle \bigstar_k^{-1} \mathsf{w}, \sigma \right\rangle = \frac{1}{|*\sigma|} \langle \mathsf{w}, *\sigma \rangle \quad \forall \sigma \in \mathcal{T}^k.$$

Note that $\bigstar_k$ is represented by a *diagonal* matrix.

Definition 3.7 (Discrete Codifferential)
The discrete codifferential $\delta_{k+1}^{\mathrm{DEC}} : C^{k+1}(\mathcal{T}) \to C^k(\mathcal{T})$ *is defined as*

$$\delta_{k+1}^{\mathrm{DEC}} := (-1)^{k+1} \star_k^{-1} \tilde{\partial}^{n-(k+1)} \star_{k+1},$$

where $\tilde{\partial}^{n-(k+1)}$ *denotes the coboundary operator on* $C^{n-(k+1)}(\tilde{\mathcal{T}})$.

As we are working with a dual mesh, we can freely write

$$\delta_{k+1}^{\mathrm{DEC}} = \star_k^{-1} \left(\partial^k\right)^T \star_{k+1}$$

by Definition 3.5, which now resembles the terms in the upper triangular part of (3.2).

In analogy to (1.1) we set

$$\mathrm{d}^{\mathrm{DEC}} := \begin{pmatrix} 0 & & & \\ \partial^0 & 0 & & \\ & \partial^1 & 0 & \\ & & \ddots & \ddots \end{pmatrix}, \quad \delta^{\mathrm{DEC}} := \begin{pmatrix} 0 & \star_0^{-1} \left(\partial^0\right)^T \star_1 & & \\ & 0 & \star_1^{-1} \left(\partial^1\right)^T \star_2 & \\ & & 0 & \ddots \\ & & & \ddots \end{pmatrix}. \tag{3.3}$$

3.3 Hodge-Dirac with DEC

In this section we endeavor to establish the discrete equivalent of the Hodge-Dirac problem in the context of DEC. For this section we will use the convention that $C \geq 0$ denotes a generic constant which may change from expression to expression and which depends only on the shape-regularity of the mesh.

3.3.1 DEC Discretization of the Hodge-Dirac Operator

Definition 3.8 ([12, Section 4.5])
For $\mathsf{u}, \mathsf{v} \in C^k(\mathcal{T})$, *define the inner product*

$$[\![\mathsf{u}, \mathsf{v}]\!]_k := \sum_{\sigma \in \mathcal{T}^k} \frac{|*\sigma|}{|\sigma|} \langle \mathsf{u}, \sigma \rangle \langle \mathsf{v}, \sigma \rangle, \tag{3.4}$$

where $\langle \mathsf{u}, \sigma \rangle \equiv \mathsf{u}(\sigma)$ *is the duality pairing of* $C^k(\mathcal{T})$ *and* $\mathcal{T}^k$. *We denote the norm induced by this inner product by* $|||\cdot|||_k$. *Let* $C(\mathcal{T}) := \bigoplus_k C^k(\mathcal{T})$ *and define an inner product thereon for* $\mathbf{u}, \mathbf{v} \in C(\mathcal{T})$ *by*

$$[\![\mathbf{u}, \mathbf{v}]\!] := \sum_{k=0}^{n} [\![\mathsf{u}_k, \mathsf{v}_k]\!]_k,$$

where $\mathbf{u} = (\mathsf{u}_0, \ldots, \mathsf{u}_n), \mathsf{u}_k \in C^k(\mathcal{T})$. *For the induced norm we write* $|||\cdot|||$.
Furthermore, let

$$[\![\cdot, \cdot]\!]_{H\Lambda(\Omega)} := [\![\cdot, \cdot]\!] + \left[\!\left[\mathrm{d}^{\mathrm{DEC}} \cdot, \mathrm{d}^{\mathrm{DEC}} \cdot\right]\!\right]$$

and denote the norm induced by this inner product by $|||\cdot|||_{H\Lambda(\Omega)}$.

Definition 3.9
Define $\mathrm{M}_k^{\mathrm{DEC}}$ *as the mass matrix of* $\mathring{C}^k(\mathcal{T})$ *w.r.t. the inner product* $[\![\cdot,\cdot]\!]_k$ *and* $\mathrm{M}^{\mathrm{DEC}}$ *as the one of* $\mathring{C}(\mathcal{T})$ *with* $[\![\cdot,\cdot]\!]$.

Note that these mass matrices are just representations of the discrete Hodge stars from Definition 3.6 and thus are diagonal.

Lemma 3.10 (Discrete Adjoint)
It holds that

$$\left[\!\left[\delta^{\mathrm{DEC}}\mathbf{u},\mathbf{v}\right]\!\right] = \left[\!\left[\mathbf{u},\mathrm{d}^{\mathrm{DEC}}\mathbf{v}\right]\!\right] \quad \forall \mathbf{u},\mathbf{v} \in \mathring{C}(\mathcal{T}).$$

Proof This follows from the definition of $[\![\cdot,\cdot]\!]$ and a proof completely analogous to [12, Lemma 4.12] (applied to cochains instead of Whitney forms). □

Definition 3.11
The DEC Hodge-Dirac operator is

$$\mathrm{D}^{\mathrm{DEC}} := \mathrm{d}^{\mathrm{DEC}} + \delta^{\mathrm{DEC}}.$$

We define an associated bilinear form on $\mathring{C}(\mathcal{T}) \times \mathring{C}(\mathcal{T})$ *by*

$$\mathcal{A}_{\mathrm{DEC}}(\cdot,\cdot) := \left[\!\left[\mathrm{d}^{\mathrm{DEC}}\cdot,\cdot\right]\!\right] + \left[\!\left[\cdot,\mathrm{d}^{\mathrm{DEC}}\cdot\right]\!\right],$$

which is represented by the matrix $A^{\mathrm{DEC}} := \mathrm{M}^{\mathrm{DEC}}\mathrm{D}^{\mathrm{DEC}}$.

Remark 3.12 *Note that* $\mathrm{D}^{\mathrm{DEC}}\mathbf{u} = \mathbf{f}$ *for* $\mathbf{u},\mathbf{f} \in \mathring{C}(\mathcal{T})$ *is equivalent to*

$$\mathcal{A}_{\mathrm{DEC}}(\mathbf{u},\mathbf{v}) = [\![\mathbf{f},\mathbf{v}]\!] \quad \forall \mathbf{v} \in \mathring{C}(\mathcal{T}), \tag{3.5}$$

i.e. a mass-lumped version of (1.5) *when discretized with Whitney forms.*

One can also look at a slightly more general form for $\tilde{\mathbf{f}} \in \mathring{C}(\mathcal{T})$

$$\mathcal{A}_{\mathrm{DEC}}(\mathbf{u},\mathbf{v}) = \left[\!\left[\tilde{\mathbf{f}},\mathbf{v}\right]\!\right]_{H\Lambda(\Omega)} \quad \forall \mathbf{v} \in \mathring{C}(\mathcal{T}). \tag{3.6}$$

(3.5) *can be transformed into* (3.6) *by the Riesz representation theorem: it tells us about the existence and uniqueness of an* $\tilde{\mathbf{f}}$ *such that* $[\![\mathbf{f},\cdot]\!] \equiv \left[\!\left[\tilde{\mathbf{f}},\cdot\right]\!\right]_{H\Lambda(\Omega)}$. *Moreover,*

$$|||\tilde{\mathbf{f}}|||_{H\Lambda(\Omega)} = \sup_{|||\mathbf{v}|||_{H\Lambda(\Omega)}=1} \left|\left[\!\left[\tilde{\mathbf{f}},\mathbf{v}\right]\!\right]_{H\Lambda(\Omega)}\right| = \sup_{|||\mathbf{v}|||_{H\Lambda(\Omega)}=1} |[\![\mathbf{f},\mathbf{v}]\!]| \leq |||\mathbf{f}|||. \tag{3.7}$$

The motivation behind it is the variational formulation (1.4). *It has a right-hand-side functional which is bounded in* $L^2\Lambda(\Omega)$. *If we instead have a linear functional bounded in* $H\Lambda(\Omega)$, *existence and uniqueness follow from the inf-sup inequality in [19, Theorem 6] (see also [3]). As we are working with Hilbert spaces, we can express a linear functional* ℓ *on* $H\Lambda(\Omega)$ *as* $\ell \equiv \langle \mathfrak{f},\cdot\rangle_{H\Lambda(\Omega)} = \langle \mathfrak{f},\cdot\rangle_{L^2\Lambda(\Omega)} + \langle \mathrm{d}\mathfrak{f},\mathrm{d}\cdot\rangle_{L^2\Lambda(\Omega)}$ *for some* $\mathfrak{f} \in H\Lambda(\Omega)$. (3.6) *is the discrete version of this.*

This setting is useful because it yields a problem which for a given $\mathfrak{f} \in \mathring{\mathfrak{V}}$ *yields another element in the same space, allowing us to interpret the solution operator as an automorphism. Also, due to* (3.7), *stability of* (3.6) *implies stability* (3.5), *hence stability of* (3.6) *is stronger than the one of* (3.5).

3.3.2 Stability of DEC

As before, we consider the boundary value problem for the Hodge-Dirac operator with essential boundary conditions, so assume that D acts on spaces with *zero trace* or *zero mean* in the case of n-forms. This also means that $\mathfrak{f} \in \operatorname{ran} \mathrm{D} \implies \int_\Omega f_n = 0$.

New in this section, now we regard $\mathcal{T}$ as a member of a *uniformly shape-regular* sequence $(\mathcal{T}_h)$ of simplicial meshes of Ω indexed by their mesh-widths h, which are supposed to tend to zero.

So far, we have not specified what kind of dual mesh we are using, so the statements up until here hold in a generic context. However, in order to establish stability, we need some assumptions on the dual mesh, or more precisely, the norm induced by the discrete Hodge star.

Assumption 3.3.1 (h-uniform Norm Equivalence)
The norms $|||\cdot|||$ and $\|\cdot\|_{L^2\Lambda^k(\Omega)}$ on spaces of cochains and Whitney forms are h-uniformly equivalent via the $\mathcal{W}$-isomorphism. More precisely, there exist constants $c_-, c_+ > 0$ depending only on the shape-regularity of $\mathcal{T}$, such that

$$c_- \|\mathcal{W}\mathbf{u}\|_{L^2\Lambda(\Omega)} \leq |||\mathbf{u}||| \leq c_+ \|\mathcal{W}\mathbf{u}\|_{L^2\Lambda(\Omega)} \quad \forall \mathbf{u} \in C(\mathcal{T}).$$

Similar to [12, Lemma 5.11], we will need the following result relating to the Hodge-decomposition (in the case of a trivial topology):

Lemma 3.13
For any $\mathbf{u} \in \mathring{C}(\mathcal{T})$ there exist $\mathbf{v}, \mathbf{w} \in \mathring{C}(\mathcal{T})$ such that

$$\begin{aligned} \mathbf{u} &= \mathrm{d}^{\mathrm{DEC}}\mathbf{v} + \mathbf{w}, \\ |||\mathbf{w}||| + \left|\left|\left|\mathrm{d}^{\mathrm{DEC}}\mathbf{w}\right|\right|\right| &\leq C\left|\left|\left|\mathrm{d}^{\mathrm{DEC}}\mathbf{u}\right|\right|\right|, \\ |||\mathbf{v}||| + \left|\left|\left|\mathrm{d}^{\mathrm{DEC}}\mathbf{v}\right|\right|\right| &\leq C'|||\mathbf{u}||| \end{aligned}$$

for constants $C, C' \geq 0$ independent of $\mathbf{u}$ and the mesh-width h.

Proof First, we note that due to the norm equivalence from Assumption 3.3.1 and the fact that $\mathcal{W}\mathrm{d}^{\mathrm{DEC}} \equiv \mathrm{d}\mathcal{W}$, it is sufficient to prove that $\exists \alpha, \beta \in \mathring{V}^h$ such that

$$\mathcal{W}\mathbf{u} = \mathrm{d}\alpha + \beta, \tag{3.8}$$

$$\|\beta\|_{L^2\Lambda(\Omega)} + \|\mathrm{d}\beta\|_{L^2\Lambda(\Omega)} \leq C\|\mathrm{d}\mathcal{W}\mathbf{u}\|_{L^2\Lambda(\Omega)}, \tag{3.9}$$

$$\|\alpha\|_{L^2\Lambda(\Omega)} + \|\mathrm{d}\alpha\|_{L^2\Lambda(\Omega)} \leq C'\|\mathcal{W}\mathbf{u}\|_{L^2\Lambda(\Omega)}. \tag{3.10}$$

To see this, we consider the discrete Hodge decomposition (see [19, Section 3.1]; recall that $\mathring{V}^h$ excludes harmonic forms)

$$\mathring{V}^h = \mathfrak{B}_h \oplus \mathfrak{Z}_h^\perp,$$

where $\mathfrak{B}_h$ is the range and $\mathfrak{Z}_h$ the kernel of $\mathrm{d}|_{\mathring{V}_h}$. Moreover, this decomposition is $L^2\Lambda(\Omega)$-orthogonal.

This implies that we can find $\alpha \in \mathring{V}^h, \beta \in \mathfrak{Z}_h^\perp$ such that $\mathcal{W}\mathbf{u} = \mathrm{d}\alpha + \beta$. Note that α is not unique, as adding any element in $\mathfrak{Z}_h$ gives the same $\mathrm{d}\alpha$, hence we can safely assume that there exists an α orthogonal to $\mathfrak{Z}_h$, meaning we can find suitable $\alpha, \beta \in \mathfrak{Z}_h^\perp$.

We can now apply the discrete Poincaré inequality from [19, Lemma 9] (see also [2, Theorem 5.2]) to β, which is applicable as $\beta \in \mathfrak{Z}_h^\perp$, and get

$$\begin{aligned}
\|\beta\|_{L^2\Lambda(\Omega)} + \|\mathrm{d}\beta\|_{L^2\Lambda(\Omega)} &\leq C\|\mathrm{d}\beta\|_{L^2\Lambda(\Omega)} && \text{[Poincaré Inequality]}\\
&= C\|\mathrm{d}\left(\mathcal{W}\mathbf{u} - \mathrm{d}\alpha\right)\|_{L^2\Lambda(\Omega)} && \text{[Using (3.8)]}\\
&= C\|\mathrm{d}\mathcal{W}\mathbf{u}\|_{L^2\Lambda(\Omega)} && \left[\mathrm{d}^2 \equiv 0\right]
\end{aligned}$$

for some mesh-width independent $C \geq 0$, which proves (3.9).

To prove (3.10), we can apply the Poincaré inequality to $\alpha \in \mathfrak{Z}_h^\perp$ and use the orthogonality of the decomposition to arrive at

$$\begin{aligned}
\|\alpha\|^2_{L^2\Lambda(\Omega)} + \|\mathrm{d}\alpha\|^2_{L^2\Lambda(\Omega)} &\leq C'\|\mathrm{d}\alpha\|^2_{L^2\Lambda(\Omega)}\\
&\leq C'\left(\|\mathrm{d}\alpha\|^2_{L^2\Lambda(\Omega)} + \|\beta\|^2_{L^2\Lambda(\Omega)}\right) = C'\|\mathcal{W}\mathbf{u}\|^2_{L^2\Lambda(\Omega)}.
\end{aligned}$$

Applying Young's inequality to the above concludes the proof. □

Lemma 3.14 (DEC Hodge-Decomposition)
Let $\mathfrak{Z}^{\mathrm{DEC}} := \ker \mathrm{d}^{\mathrm{DEC}}$, $\mathfrak{B}^{\mathrm{DEC}} := \operatorname{ran} \mathrm{d}^{\mathrm{DEC}}$, $\mathfrak{H}^{\mathrm{DEC}} := \ker \mathrm{D}^{\mathrm{DEC}}$, *then we have the DEC-orthogonal (i.e. orthogonal w.r.t.* $[\![\cdot,\cdot]\!]$*) decomposition*

$$\mathring{C}\left(\mathcal{T}\right) = \mathfrak{B}^{\mathrm{DEC}} \oplus \left(\mathfrak{Z}^{\mathrm{DEC}}\right)^{\perp_{\mathrm{DEC}}} \oplus \mathfrak{H}^{\mathrm{DEC}},$$

where $\perp_{\mathrm{DEC}}$ *means orthogonal w.r.t.* $[\![\cdot,\cdot]\!]$.

Proof The statement is a consequence of [19, Section 2.1], as we are in the same setting because $\mathrm{d}^{\mathrm{DEC}}$ is nilpotent and adjoint to δ^{DEC} by Lemma 3.10.

Note that due to the trivial topology $\ker \mathrm{D}^{\mathrm{DEC}} \equiv \mathfrak{H}^{\mathrm{DEC}}$ is trivial and can be dropped.

Lemma 3.15 (Poincaré Inequality for DEC)
Given $\mathbf{u} \in \left(\mathfrak{Z}^{\mathrm{DEC}}\right)^{\perp_{\mathrm{DEC}}}$ *it holds that*

$$|||\mathbf{u}|||_{H\Lambda(\Omega)} \leq c_p \left|\left|\left|\mathrm{d}^{\mathrm{DEC}}\mathbf{u}\right|\right|\right|$$

for some mesh-width independent constant $c_p \geq 1$.

Proof We first invoke Lemma 3.13 to find $\mathbf{v}, \mathbf{w} \in \mathring{C}\left(\mathcal{T}\right)$ such that

$$\mathbf{u} = \mathrm{d}^{\mathrm{DEC}}\mathbf{v} + \mathbf{w}, \qquad |||\mathbf{w}||| \leq C\left|\left|\left|\mathrm{d}^{\mathrm{DEC}}\mathbf{u}\right|\right|\right|$$

and then apply Lemma 3.14 to $\mathbf{w}$, which implies the *orthogonal* decomposition

$$\mathbf{w} = \mathrm{d}^{\mathrm{DEC}}\tilde{\mathbf{v}} + \tilde{\mathbf{w}},$$

for some $\tilde{\mathbf{v}} \in \mathring{C}\left(\mathcal{T}\right), \tilde{\mathbf{w}} \in \left(\mathfrak{Z}^{\mathrm{DEC}}\right)^{\perp_{\mathrm{DEC}}}$. This gives us the following form of the Hodge decomposition of $\mathbf{u}$:

$$\mathbf{u} = \mathrm{d}^{\mathrm{DEC}}\mathbf{v} + \mathbf{w} = \mathrm{d}^{\mathrm{DEC}}\left(\mathbf{v} + \tilde{\mathbf{v}}\right) + \tilde{\mathbf{w}},$$

but the assumption of the lemma was that $\mathbf{u} \in \left(\mathfrak{Z}^{\mathrm{DEC}}\right)^{\perp_{\mathrm{DEC}}}$, thus $\tilde{\mathbf{w}} = \mathbf{u}$ must hold by uniqueness of the decomposition.

We realize that due to orthogonality, we have

$$|||\mathbf{u}||| = |||\tilde{\mathbf{w}}||| \leq |||\mathbf{w}||| \leq C\left|\left|\left|\mathrm{d}^{\mathrm{DEC}}\mathbf{u}\right|\right|\right|,$$

which implies $|||\mathbf{u}|||_{H\Lambda(\Omega)} \leq C\left|\left|\left|\mathrm{d}^{\mathrm{DEC}}\mathbf{u}\right|\right|\right|$, concluding the proof. □

Proposition 3.16 (DEC Inf-Sup Inequality, [19, Theorem 6])
There exists a constant $\gamma > 0$ depending only on the Poincaré constant, such that for all nonzero $\mathbf{u} \in \mathring{C}(\mathcal{T})$, there exists a nonzero $\mathbf{v} \in \mathring{C}(\mathcal{T})$ satisfying

$$\gamma|||\mathbf{u}|||_{H\Lambda(\Omega)}|||\mathbf{v}|||_{H\Lambda(\Omega)} \leq \mathcal{A}_{\mathrm{DEC}}(\mathbf{u},\mathbf{v}).$$

Proof The proof is almost the same as the one from [19, Theorem 6], but with the norms replaced by the DEC norms. We will go through it for completeness' sake.

Take the Hodge decomposition of

$$\mathbf{u} = \mathrm{d}^{\mathrm{DEC}}\mathbf{r} + \mathbf{w}$$

with $\mathbf{r} \in \left(\mathfrak{Z}^{\mathrm{DEC}}\right)^{\perp_{\mathrm{DEC}}}$ and define $\mathbf{v} := \mathbf{r} + \mathrm{d}^{\mathrm{DEC}}\mathbf{u}$.

The Poincaré inequality for DEC from Lemma 3.15 together with the orthogonality of the Hodge decomposition from Lemma 3.14 yields

$$\begin{aligned}
|||\mathbf{v}|||_{H\Lambda(\Omega)} &\leq |||\mathbf{r}|||_{H\Lambda(\Omega)} + \left|\left|\left|\mathrm{d}^{\mathrm{DEC}}\mathbf{u}\right|\right|\right|_{H\Lambda(\Omega)} \\
&\leq c_p\left|\left|\left|\mathrm{d}^{\mathrm{DEC}}\mathbf{r}\right|\right|\right| + \left|\left|\left|\mathrm{d}^{\mathrm{DEC}}\mathbf{u}\right|\right|\right| \\
&\leq C|||\mathbf{u}|||_{H\Lambda(\Omega)},
\end{aligned} \tag{3.11}$$

where we used that $\left|\left|\left|\mathrm{d}^{\mathrm{DEC}}\mathbf{u}\right|\right|\right|_{H\Lambda(\Omega)} = \left|\left|\left|\mathrm{d}^{\mathrm{DEC}}\mathbf{u}\right|\right|\right|$.
Substituting this into the bilinear form and once again using the Hodge decomposition and Poincaré inequality gives

$$\begin{aligned}
\mathcal{A}_{\mathrm{DEC}}(\mathbf{u},\mathbf{v}) &= \left|\left|\left|\mathrm{d}^{\mathrm{DEC}}\mathbf{u}\right|\right|\right|^2 + \left[\!\left[\mathbf{u}, \mathrm{d}^{\mathrm{DEC}}\mathbf{r}\right]\!\right] \\
&= \left|\left|\left|\mathrm{d}^{\mathrm{DEC}}\mathbf{u}\right|\right|\right|^2 + \left[\!\left[\mathrm{d}^{\mathrm{DEC}}\mathbf{r}, \mathrm{d}^{\mathrm{DEC}}\mathbf{r}\right]\!\right] \\
&= \frac{1}{2}\left|\left|\left|\mathrm{d}^{\mathrm{DEC}}\mathbf{u}\right|\right|\right|^2 + \frac{1}{2}\left|\left|\left|\mathrm{d}^{\mathrm{DEC}}\mathbf{w}\right|\right|\right|^2 + \left|\left|\left|\mathrm{d}^{\mathrm{DEC}}\mathbf{r}\right|\right|\right|^2 \\
&\geq \frac{1}{2}\left|\left|\left|\mathrm{d}^{\mathrm{DEC}}\mathbf{u}\right|\right|\right|^2 + \frac{1}{2c_p^2}|||\mathbf{w}|||^2 + \left|\left|\left|\mathrm{d}^{\mathrm{DEC}}\mathbf{r}\right|\right|\right|^2 \\
&\geq \frac{1}{2c_p^2}|||\mathbf{u}|||^2_{H\Lambda(\Omega)},
\end{aligned}$$

where the last inequality follows from $c_p \geq 1$. Combining this with (3.11) yields the statement. □

Corollary 3.17 (Stability of DEC)
Let $\mathbf{f} \in \mathring{C}(\mathcal{T})$ *be given and let* $\mathbf{u} \in \mathring{C}(\mathcal{T})$ *be the solution to*

$$\mathcal{A}_{\mathrm{DEC}}(\mathbf{u}, \mathbf{v}) = [\![\mathbf{f}, \mathbf{v}]\!]_{H\Lambda(\Omega)} \quad \forall \mathbf{v} \in \mathring{C}(\mathcal{T}),$$

then

$$|||\mathbf{u}|||_{H\Lambda(\Omega)} \leq C|||\mathbf{f}|||_{H\Lambda(\Omega)}$$

for some constant $C \geq 0$ *independent of* $\mathbf{f}$ *and the mesh-width.*

Proof This follows from Cauchy-Schwarz and Proposition 3.16: Let $\mathbf{v}$ be given by applying Proposition 3.16 to $\mathbf{u}$, then

$$\gamma|||\mathbf{u}|||_{H\Lambda(\Omega)}|||\mathbf{v}|||_{H\Lambda(\Omega)} \leq \mathcal{A}_{\mathrm{DEC}}(\mathbf{u}, \mathbf{v}) = [\![\mathbf{f}, \mathbf{v}]\!]_{H\Lambda(\Omega)} \leq |||\mathbf{f}|||_{H\Lambda(\Omega)}|||\mathbf{v}|||_{H\Lambda(\Omega)},$$

which implies the statement. □

3.3.3 Spectral Equivalence to FEEC

In [16], an abstract approach to bounding the spectral condition numbers of problems arising from bilinear forms fulfilling an inf-sup condition is elucidated. As both the DEC and FEEC bilinear forms fulfill such inf-sup inequalities, and since both bilinear forms are bounded h-uniformly in the Sobolev norms, we may employ similar means to prove spectral equivalence.

Notice that A^{DEC} and A^{FEEC} do not necessarily map to vectors of coefficients fulfilling the zero mean condition. Instead, we can to understand them as the matrices representing the induced operators of the bilinear forms $\mathcal{A}_{\mathrm{DEC}}(\cdot,\cdot) := [\![\mathrm{d}\cdot, \cdot]\!] + [\![\cdot, \mathrm{d}\cdot]\!]$ and $\mathcal{A}_{\mathrm{FEEC}}(\cdot,\cdot) := \langle \mathrm{d}\cdot, \cdot\rangle_{L^2\Lambda(\Omega)} + \langle \cdot, \mathrm{d}\cdot\rangle_{L^2\Lambda(\Omega)}$, respectively, i.e.

$$\begin{aligned} B^{\mathrm{FEEC}}: \quad \mathring{V}^h \quad &\to \quad \left(\mathring{V}^h\right)^*, \\ B^{\mathrm{DEC}}: \quad \mathring{C}(\mathcal{T}) \quad &\to \quad \left(\mathring{C}(\mathcal{T})\right)^*, \end{aligned}$$

where the $*$ denotes the dual vector space. As norms on the spaces we use the respective Sobolev norms and the norms induced thereby on the dual spaces.

Using the Whitney isomorphism, we see that

$$T := \mathcal{W}^{-1}\left(B^{\mathrm{DEC}}\right)^{-1}\mathcal{W}B^{\mathrm{FEEC}} : \mathring{V}^h \to \mathring{V}^h$$

is a well-defined automorphism on $\mathring{V}^h$, represented by the matrix $\left(A^{\mathrm{DEC}}\right)^{-1}A^{\mathrm{FEEC}}$[1].

Lemma 3.18 (FEEC Inf-Sup Inequality, [19, Theorem 10])
There exists a constant $\gamma > 0$ *depending only on the Poincaré constant, such that for all nonzero* $u_h \in \mathring{V}^h$*, there exists a nonzero* $v_h \in \mathring{V}^h$ *satisfying*

$$\gamma\|u_h\|_{H\Lambda(\Omega)}\|v_h\|_{H\Lambda(\Omega)} \leq \mathcal{A}_{\mathrm{FEEC}}(u_h, v_h).$$

[1] Note that the matrices by themselves are not invertible without incorporating the zero mean condition somewhere. Also important to mention is that while the dual spaces may be isomorphic to the vector spaces themselves, the zero mean condition on the duals may not manifest as a a simple sum-zero requirement on the corresponding coefficients as for $\mathring{C}(\mathcal{T}), \mathring{V}^h$.

Lemma 3.19 (*h*-uniform Boundedness of Bilinear Forms and Inverses)
It holds that

$$\begin{aligned} \left|\left|\left| B^{\mathrm{DEC}} \right|\right|\right|_{\mathring{C}(\mathcal{T})\to\left(\mathring{C}(\mathcal{T})\right)^*} &, \quad \left\| B^{\mathrm{FEEC}} \right\|_{\mathring{V}^h\to\left(\mathring{V}^h\right)^*}, \\ \left|\left|\left| \left(B^{\mathrm{DEC}}\right)^{-1} \right|\right|\right|_{\left(\mathring{C}(\mathcal{T})\right)^*\to\mathring{C}(\mathcal{T})} &, \quad \left\| \left(B^{\mathrm{FEEC}}\right)^{-1} \right\|_{\left(\mathring{V}^h\right)^*\to\mathring{V}^h} \end{aligned}$$

are all bounded from above by constants independent of the mesh-width.

Proof For the FEEC problem, we immediately see that

$$\mathcal{A}_{\mathrm{FEEC}}(u_h, v_h) \leq 2\|u_h\|_{H\Lambda(\Omega)}\|v_h\|_{H\Lambda(\Omega)} \quad \forall u_h, v_h \in \mathring{V}^h$$

which implies $\left\| B^{\mathrm{FEEC}} \right\|_{\mathring{V}^h\to\left(\mathring{V}^h\right)^*} \leq 2$.
Proposition 3.16 implies that $\left|\left|\left| \left(B^{\mathrm{DEC}}\right)^{-1} \right|\right|\right|_{\left(\mathring{C}(\mathcal{T})\right)^*\to\mathring{C}(\mathcal{T})} \leq C$.

For the DEC problem, we have

$$\mathcal{A}_{\mathrm{DEC}}(\mathbf{u}, \mathbf{v}) \leq 2|||\mathbf{u}|||_{H\Lambda(\Omega)}|||\mathbf{v}|||_{H\Lambda(\Omega)} \quad \forall \mathbf{u}, \mathbf{v} \in \mathring{C}(\mathcal{T})$$

which implies $\left|\left|\left| B^{\mathrm{DEC}} \right|\right|\right|_{\mathring{C}(\mathcal{T})\to\left(\mathring{C}(\mathcal{T})\right)^*} \leq 2$.
Lemma 3.18 implies $\left\| \left(B^{\mathrm{FEEC}}\right)^{-1} \right\|_{\left(\mathring{V}^h\right)^*\to\mathring{V}^h} \leq C$, concluding the proof. □

Theorem 3.20 (Spectral Equivalence of DEC and FEEC)
Let

$$\kappa(A) := \|A\|_{\mathring{V}^h\to\mathring{V}^h}\left\|A^{-1}\right\|_{\mathring{V}^h\to\mathring{V}^h}$$

denote the spectral condition number of an automorphism $A : \mathring{V}^h \to \mathring{V}^h$ and $\rho(A)$ the spectral radius, then

$$\kappa(T) \leq c, \quad \rho(T) \leq c', \quad \rho\left(T^{-1}\right) \leq c''$$

for some mesh-width independent constants $c, c', c'' \geq 0$.

Proof We first note that due to Assumption 3.3.1, we have

$$\|T\|_{\mathring{V}^h\to\mathring{V}^h} \leq C\left|\left|\left| \left(B^{\mathrm{DEC}}\right)^{-1} \right|\right|\right|_{\left(\mathring{C}(\mathcal{T})\right)^*\to\mathring{C}(\mathcal{T})}\left\| B^{\mathrm{FEEC}} \right\|_{\mathring{V}^h\to\left(\mathring{V}^h\right)^*}.$$

and

$$\left\|T^{-1}\right\|_{\mathring{V}^h\to\mathring{V}^h} \leq C\left|\left|\left| B^{\mathrm{DEC}} \right|\right|\right|_{\mathring{C}(\mathcal{T})\to\left(\mathring{C}(\mathcal{T})\right)^*}\left\| \left(B^{\mathrm{FEEC}}\right)^{-1} \right\|_{\left(\mathring{V}^h\right)^*\to\mathring{V}^h}.$$

The estimate on the condition number is then a trivial consequence of Lemma 3.19. The eigenvalues can be bounded from above by the operator norms, so the estimates on $\rho(T), \rho\left(T^{-1}\right)$ follow immediately, which concludes the proof. □

3.3.4 Commuting Interpolation Operators

From the results in [12, Section 4] (cf. [7, Proposition 5.5]) we learn the following commuting diagram property.

Lemma 3.21
On sufficiently smooth forms, we have the commuting relationship

$$\mathrm{d}^{\mathrm{DEC}} \circ \mathcal{R} = \mathcal{R} \circ \mathrm{d}.$$

Definition 3.22 ([12, Section 5.1])
Let $J_k := \star_k^{-1} \tilde{\mathcal{R}}^{n-k} \star_k$, *where* $\tilde{\mathcal{R}}^k$ *denotes the canonical projection onto* $C^k\left(\tilde{\mathcal{T}}\right)$, *and define* $J := \bigoplus_k J_k$.

Lemma 5.3 of [12] asserts another commuting property.

Lemma 3.23
On sufficiently smooth forms, we have the commuting relationship

$$\delta^{\mathrm{DEC}} \circ J = J \circ \delta.$$

The natural DEC discretization of (1.3) is: Given $\mathfrak{f} \in L^2\Lambda\left(\Omega\right)$ with $\int_\Omega f_n = 0$ which is sufficiently regular to admit an L^1-trace on all simplices, seek $\mathbf{u} \in \mathring{C}\left(\mathcal{T}\right)$, such that

$$\mathrm{D}^{\mathrm{DEC}}\mathbf{u} = \mathcal{R}\mathfrak{f}. \tag{3.12}$$

We need $\int_\Omega f_n = 0$ also in the discrete case, because we want $\mathcal{R}\mathfrak{f} \in \operatorname{ran}\mathrm{D}^{\mathrm{DEC}}$, but $\operatorname{ran}\mathrm{D}^{\mathrm{DEC}}$ only contains n-cochains with zero mean. The de Rham map $\mathcal{R}$ preserves the integral of the traces over the simplices, so we get $\mathcal{R}\mathfrak{f} \in \operatorname{ran}\mathrm{D}^{\mathrm{DEC}}$.

3.3.5 Error Bound

Theorem 3.24
Given $\mathfrak{f} \in \operatorname{ran}\mathrm{D}$ *in the domain of* $\mathcal{R}$ *and* J, *we assume that the strong solution* $\mathfrak{u} \in \mathring{\mathfrak{V}} \cap H^*\Lambda\left(\Omega\right)$ *of the Hodge-Dirac boundary value problem*

$$\mathrm{D}\mathfrak{u} = \mathfrak{f}$$

is sufficiently regular such that Lemma 3.21 and Lemma 3.23 apply and $\mathcal{R}$ *and* J *are well-defined on* $\mathfrak{u}, \mathrm{d}\mathfrak{u}$ *and* $\delta\mathfrak{u}$. *Further let* $\mathbf{u} \in \mathring{C}\left(\mathcal{T}\right)$ *solve the DEC equation*

$$\mathrm{D}^{\mathrm{DEC}}\mathbf{u} = \mathcal{R}\mathfrak{f},$$

and denote the error in cochain space by $e := \mathcal{R}\mathfrak{u} - \mathbf{u}$. *Then*

$$|||e||| + \left|\left|\left|\mathrm{d}^{\mathrm{DEC}}e\right|\right|\right| \leq C\left(|||(\mathcal{R}-J)\mathfrak{u}||| + |||(\mathcal{R}-J)\mathrm{d}\mathfrak{u}||| + |||(\mathcal{R}-J)\mathfrak{f}|||\right),$$

where $C \geq 0$ *is a constant independent of* $\mathfrak{f}$ *and the mesh-width* h.

Proof Unless stated otherwise, $C, C' \geq 0$ denote generic mesh-width independent constants which may change from expression to expression.

Similar to the proof of Theorem 5.2 in [12], we apply the operator to the error e and get an estimate of $\left|\left|\left|\mathrm{d}^{\mathrm{DEC}}e\right|\right|\right|$:

$$
\begin{aligned}
\mathrm{D}^{\mathrm{DEC}} e &= (\mathrm{d}^{\mathrm{DEC}} + \delta^{\mathrm{DEC}}) e && \text{[Definition 3.11]} \\
&= \mathrm{d}^{\mathrm{DEC}} \mathcal{R}\mathfrak{u} + \delta^{\mathrm{DEC}} \mathcal{R}\mathfrak{u} - (\mathrm{d}^{\mathrm{DEC}} + \delta^{\mathrm{DEC}})\mathbf{u} && [e = \mathcal{R}\mathfrak{u} - \mathbf{u}] \\
&= \mathrm{d}^{\mathrm{DEC}} \mathcal{R}\mathfrak{u} + \delta^{\mathrm{DEC}} \mathcal{R}\mathfrak{u} - \mathcal{R}\mathfrak{f} && \left[\text{Using } (\mathrm{d}^{\mathrm{DEC}} + \delta^{\mathrm{DEC}})\mathbf{u} = \mathcal{R}\mathfrak{f}\right] \\
&= \mathcal{R}\mathrm{d}\mathfrak{u} + \delta^{\mathrm{DEC}} J\mathfrak{u} + \delta^{\mathrm{DEC}}(\mathcal{R} - J)\mathfrak{u} - \mathcal{R} f && \text{[Adding 0, Lemma 3.21]} \\
&= (\mathcal{R} - J)\mathrm{d}\mathfrak{u} + \delta^{\mathrm{DEC}}(\mathcal{R} - J)\mathfrak{u} + (J - \mathcal{R})\mathfrak{f}. && \left[\text{Using } \delta^{\mathrm{DEC}} J\mathfrak{u} = J\delta\mathfrak{u} = J(\mathfrak{f} - \mathrm{d}\mathfrak{u})\right]
\end{aligned} \tag{3.13}
$$

$$
\begin{aligned}
\implies \quad \delta^{\mathrm{DEC}} \mathrm{d}^{\mathrm{DEC}} e &= \delta^{\mathrm{DEC}} (\mathrm{d}^{\mathrm{DEC}} + \delta^{\mathrm{DEC}}) e && \left[\text{Using } \left(\delta^{\mathrm{DEC}}\right)^2 = 0\right] \\
&= \delta^{\mathrm{DEC}} (\mathcal{R} - J)\mathrm{d}\mathfrak{u} + \delta^{\mathrm{DEC}}(J - \mathcal{R})\mathfrak{f}. \\
\implies \quad \left|\!\left|\!\left| \mathrm{d}^{\mathrm{DEC}} e \right|\!\right|\!\right|^2 &= \left[\!\left[\mathrm{d}^{\mathrm{DEC}} e, \mathrm{d}^{\mathrm{DEC}} e \right]\!\right] = \left[\!\left[\delta^{\mathrm{DEC}} \mathrm{d}^{\mathrm{DEC}} e, e \right]\!\right] && \text{[Lemma 3.10]} \\
&= \left[\!\left[\delta^{\mathrm{DEC}} (\mathcal{R} - J)\mathrm{d}\mathfrak{u} + \delta^{\mathrm{DEC}}(J - \mathcal{R})\mathfrak{f}, e \right]\!\right] && \left[\text{Using } \left(\delta^{\mathrm{DEC}}\right)^2 = 0\right] \\
&= \left[\!\left[(\mathcal{R} - J)\mathrm{d}\mathfrak{u}, \mathrm{d}^{\mathrm{DEC}} e \right]\!\right] + \left[\!\left[(J - \mathcal{R})\mathfrak{f}, \mathrm{d}^{\mathrm{DEC}} e \right]\!\right] && \text{[Lemma 3.10]} \\
&\leq |\!|\!| (\mathcal{R} - J)\mathrm{d}\mathfrak{u} |\!|\!| \left|\!\left|\!\left| \mathrm{d}^{\mathrm{DEC}} e \right|\!\right|\!\right| + |\!|\!| (J - \mathcal{R})\mathfrak{f} |\!|\!| \left|\!\left|\!\left| \mathrm{d}^{\mathrm{DEC}} e \right|\!\right|\!\right|. && \text{[Cauchy-Schwarz]} \\
\implies \quad \left|\!\left|\!\left| \mathrm{d}^{\mathrm{DEC}} e \right|\!\right|\!\right| &\leq |\!|\!| (\mathcal{R} - J)\mathrm{d}\mathfrak{u} |\!|\!| + |\!|\!| (\mathcal{R} - J)\mathfrak{f} |\!|\!|. && (3.14)
\end{aligned}
$$

To bound $|\!|\!| e |\!|\!|$, we proceed similarly to [12, Lemma 5.14]: Using Lemma 3.13, we find $\mathbf{v}, \mathbf{w} \in \mathring{\mathrm{C}}(\mathcal{T})$ such that

$$
e = \mathrm{d}^{\mathrm{DEC}} \mathbf{v} + \mathbf{w}, \quad |\!|\!| \mathbf{v} |\!|\!| + \left|\!\left|\!\left| \mathrm{d}^{\mathrm{DEC}} \mathbf{v} \right|\!\right|\!\right| \leq C |\!|\!| e |\!|\!|, \quad |\!|\!| \mathbf{w} |\!|\!| \leq C' \left|\!\left|\!\left| \mathrm{d}^{\mathrm{DEC}} e \right|\!\right|\!\right|. \tag{3.15}
$$

Thus,

$$
|\!|\!| e |\!|\!|^2 = \left[\!\left[\mathrm{d}^{\mathrm{DEC}} \mathbf{v}, e \right]\!\right] + [\![\mathbf{w}, e]\!] = \left[\!\left[\mathbf{v}, \delta^{\mathrm{DEC}} e \right]\!\right] + [\![\mathbf{w}, e]\!]
$$

by Lemma 3.10. We can immediately estimate the second term using (3.14):

$$
[\![\mathbf{w}, e]\!] \leq |\!|\!| \mathbf{w} |\!|\!| \, |\!|\!| e |\!|\!| \leq C' \left|\!\left|\!\left| \mathrm{d}^{\mathrm{DEC}} e \right|\!\right|\!\right| |\!|\!| e |\!|\!| \leq C' \left(|\!|\!| (\mathcal{R} - J)\mathrm{d}\mathfrak{u} |\!|\!| + |\!|\!| (\mathcal{R} - J)\mathfrak{f} |\!|\!| \right) |\!|\!| e |\!|\!|. \tag{3.16}
$$

In order to estimate the first term, we re-write $\delta^{\mathrm{DEC}} e$ using (3.13):

$$
\delta^{\mathrm{DEC}} e = \mathrm{D}^{\mathrm{DEC}} e - \mathrm{d}^{\mathrm{DEC}} e = \delta^{\mathrm{DEC}} (\mathcal{R} - J)\mathfrak{u} + (\mathcal{R} - J)\mathrm{d}\mathfrak{u} + (J - \mathcal{R})\mathfrak{f} - \mathrm{d}^{\mathrm{DEC}} e.
$$

$$
\begin{aligned}
\implies \left[\!\left[\mathbf{v}, \delta^{\mathrm{DEC}} e\right]\!\right] &= \left[\!\left[\mathbf{v}, \delta^{\mathrm{DEC}}(\mathcal{R}-J)\mathfrak{u} + (\mathcal{R}-J)\mathrm{d}\mathfrak{u} + (J-\mathcal{R})\mathfrak{f} - \mathrm{d}^{\mathrm{DEC}} e\right]\!\right] \\
&= \left[\!\left[\mathrm{d}^{\mathrm{DEC}}\mathbf{v}, (\mathcal{R}-J)\mathfrak{u}\right]\!\right] + [\![\mathbf{v}, (\mathcal{R}-J)\mathrm{d}\mathfrak{u}]\!] + \\
&\quad [\![\mathbf{v}, (J-\mathcal{R})\mathfrak{f}]\!] - \left[\!\left[\mathbf{v}, \mathrm{d}^{\mathrm{DEC}} e\right]\!\right] \\
&\leq \left|\!\left|\!\left|\mathrm{d}^{\mathrm{DEC}}\mathbf{v}\right|\!\right|\!\right| |\!|\!|(\mathcal{R}-J)\mathfrak{u}|\!|\!| + \\
&\quad |\!|\!|\mathbf{v}|\!|\!| \left(|\!|\!|(\mathcal{R}-J)\mathrm{d}\mathfrak{u}|\!|\!| + |\!|\!|(\mathcal{R}-J)\mathfrak{f}|\!|\!| + \left|\!\left|\!\left|\mathrm{d}^{\mathrm{DEC}} e\right|\!\right|\!\right| \right) \qquad \text{[Cauchy-Schwarz]} \\
&\leq \left|\!\left|\!\left|\mathrm{d}^{\mathrm{DEC}}\mathbf{v}\right|\!\right|\!\right| |\!|\!|(\mathcal{R}-J)\mathfrak{u}|\!|\!| + \\
&\quad 2|\!|\!|\mathbf{v}|\!|\!| \left(|\!|\!|(\mathcal{R}-J)\mathrm{d}\mathfrak{u}|\!|\!| + |\!|\!|(\mathcal{R}-J)\mathfrak{f}|\!|\!| \right) \qquad \text{[Using (3.14)]} \\
&\leq 2 \left(|\!|\!|(\mathcal{R}-J)\mathfrak{u}|\!|\!| + |\!|\!|(\mathcal{R}-J)\mathrm{d}\mathfrak{u}|\!|\!| + \right. \\
&\qquad \left. |\!|\!|(\mathcal{R}-J)\mathfrak{f}|\!|\!| \right) \left(|\!|\!|\mathbf{v}|\!|\!| + \left|\!\left|\!\left|\mathrm{d}^{\mathrm{DEC}}\mathbf{v}\right|\!\right|\!\right| \right) \\
&\leq C \left(|\!|\!|(\mathcal{R}-J)\mathfrak{u}|\!|\!| + |\!|\!|(\mathcal{R}-J)\mathrm{d}\mathfrak{u}|\!|\!| + |\!|\!|(\mathcal{R}-J)\mathfrak{f}|\!|\!| \right) |\!|\!|e|\!|\!|. \qquad \text{[Using (3.15)]} \\
& \qquad\qquad\qquad\qquad\qquad\qquad\qquad\qquad\qquad\qquad\qquad\qquad\qquad\qquad\qquad\qquad (3.17)
\end{aligned}
$$

Combining (3.16) and (3.17), we get

$$
\begin{aligned}
|\!|\!|e|\!|\!|^2 &= \left[\!\left[\mathbf{v}, \delta^{\mathrm{DEC}} e\right]\!\right] + [\![\mathbf{w}, e]\!] \\
&\leq C' \left(|\!|\!|(\mathcal{R}-J)\mathrm{d}\mathfrak{u}|\!|\!| + |\!|\!|(\mathcal{R}-J)\mathfrak{f}|\!|\!| \right) |\!|\!|e|\!|\!| + \\
&\quad C \left(|\!|\!|(\mathcal{R}-J)\mathfrak{u}|\!|\!| + |\!|\!|(\mathcal{R}-J)\mathrm{d}\mathfrak{u}|\!|\!| + |\!|\!|(\mathcal{R}-J)\mathfrak{f}|\!|\!| \right) |\!|\!|e|\!|\!|. \\
\implies |\!|\!|e|\!|\!| + \left|\!\left|\!\left|\mathrm{d}^{\mathrm{DEC}} e\right|\!\right|\!\right| &\leq C \left(|\!|\!|(\mathcal{R}-J)\mathfrak{u}|\!|\!| + |\!|\!|(\mathcal{R}-J)\mathrm{d}\mathfrak{u}|\!|\!| + |\!|\!|(\mathcal{R}-J)\mathfrak{f}|\!|\!| \right),
\end{aligned}
$$

which is the assertion of the theorem. □

Remark 3.25 *We examined the discretization error in a finite-difference sense as the difference of the discrete solution and a "projection of the exact solution on $\mathcal{T}$". We can easily obtain an error estimate in the FEEC sense:*

$$
\|\mathfrak{u} - \mathcal{W}\mathbf{u}\|_{H\Lambda(\Omega)} \leq C \left(\|\mathfrak{u} - \mathcal{W}\mathcal{R}\mathfrak{u}\|_{H\Lambda(\Omega)} + |\!|\!|e|\!|\!| + \left|\!\left|\!\left|\mathrm{d}^{\mathrm{DEC}} e\right|\!\right|\!\right| \right).
$$

3.3.6 Rates of Convergence

While we can conclude stability under the rather mild Assumption 3.3.1, we cannot conclude convergence. In order to establish convergence, we need to be more specific about the dual mesh. For this, we rely on an oriented *well-centered* simplicial mesh $\mathcal{T}$ of Ω, that is, as stipulated by [17, Definition 2.4.3] the circumcenter of any simplex of $\mathcal{T}$ lies in its interior.

For the standard dual mesh for DEC consisting of the circumcenters, see [12, Definition 3.3] or [22] for a detailed explanation, we have that

Lemma 3.26 ([12, Lemma 4.11])
Assumption 3.3.1 holds true for circumcentric duals on well-centered simplicial meshes.

[12] proves the following estimate on $\mathcal{R} - J$ in this setting.

Lemma 3.27
Given a sufficiently smooth $\mathfrak{u} \equiv (u_0, \dots, u_n)$ *in the exterior algebra of differential forms, we have*

$$|||(\mathcal{R} - J)\mathfrak{u}|||^2 \leq C \sum_{k=0}^{n} \sum_{s=1}^{r_k} h^{2s} |u_k|^2_{H^s(\Omega)},$$

where h *is the mesh-width,* $C \geq 0$ *a constant independent of* h *and* $r_k = \max \left\{ \lceil \frac{n-k}{2} + \varepsilon \rceil, \lceil \frac{k}{2} + \varepsilon \rceil \right\}$ *for any* $0 < \varepsilon < 1$.

Proof [12, Lemma 5.10] tells us that for all k, we have

$$\left|\left|\left| (\mathcal{R}^k - J_k) u_k \right|\right|\right|_k^2 \leq C_k \sum_{s=1}^{r_k} h^{2s} |u_k|^2_{H^s(\Omega)}$$

for some h-independent constant C_k. Realizing that $|||\mathbf{v}|||^2 = \sum_{k=0}^{n} |||\mathrm{v}_k|||_k^2$ for all $\mathbf{v} \in C(\mathcal{T})$ and setting $C = \max_k C_k$ yields the desired result. □

In a similar setting as before, we can prove an estimate for sufficiently smooth solutions. Let $C^\ell \Lambda(\Omega)$ denote the space of ℓ-times continuously differentiable forms.

Proposition 3.28
Let $r := \lceil \frac{n}{2} + \epsilon \rceil$ *for any* $0 < \epsilon < 1$. *Given* $\mathfrak{f} \in \operatorname{ran} \mathrm{D} \cap C^r \Lambda(\Omega)$, *assume that we are given a strong solution* $\mathfrak{u} \in \mathring{\mathfrak{V}} \cap C^{r+1} \Lambda(\Omega)$ *to the Hodge-Dirac problem*

$$\mathrm{D}\mathfrak{u} = \mathfrak{f}.$$

Let $\mathbf{u} \in \mathring{C}(\mathcal{T})$ *solve its discrete counterpart*

$$\mathrm{D}^{\mathrm{DEC}} \mathbf{u} = \mathcal{R}\mathfrak{f},$$

and denote the error in cochain space by $e := \mathcal{R}\mathfrak{u} - \mathbf{u}$. *Then*

$$|||e|||^2 + \left|\left|\left| \mathrm{d}^{\mathrm{DEC}} e \right|\right|\right|^2 \leq C \sum_{k=0}^{n} \sum_{s=1}^{r_k} h^{2s} \left(|u_k|^2_{H^s(\Omega)} + |(\mathrm{d}\mathfrak{u})_k|^2_{H^s(\Omega)} + |f_k|^2_{H^s(\Omega)} \right)$$

for some $C \geq 0$ *independent of* h *and* $r_k = \max \left\{ \lceil \frac{n-k}{2} + \varepsilon \rceil, \lceil \frac{k}{2} + \varepsilon \rceil \right\}$ *for any* $0 < \varepsilon < 1$.

Proof Let $p = |||e|||, q = \left|\left|\left| \mathrm{d}^{\mathrm{DEC}} e \right|\right|\right|, r = |||(\mathcal{R} - J)\mathfrak{u}|||, s = |||(\mathcal{R} - J)\mathrm{d}\mathfrak{u}|||, t = |||(\mathcal{R} - J)\mathfrak{f}|||$, then the estimate in Theorem 3.24 says

$$p + q \leq C(r + s + t).$$

By (repeated application of) Young's inequality and because $p, q \geq 0$, we have

$$p^2 + q^2 \leq (p + q)^2 \leq C^2(r + s + t)^2 \leq 2C^2(r^2 + (s + t)^2) \leq 4C^2(r^2 + s^2 + t^2).$$

The statement then follows from applying Lemma 3.27 to the terms r^2, t^2 and s^2. □

Remark 3.29 *The approach pursued here follows [12] very closely, but a different route could have been taken to prove convergence, at least in 2D. [28] uses a very close relationship between the inner products from FEEC and DEC (on suitable meshes) to show that the consistency gap between FEEC and DEC solutions for the Hodge-Laplacian decreases with the mesh-width, then convergence of FEEC implies convergence of DEC. The advantage of that approach is that we do not have to assume that the solution enjoys the high regularity stipulated in Proposition 3.28.*

3.4 Multigrid

We will now describe a multigrid method for the Hodge-Dirac operator in the context of DEC.

3.4.1 Transfer Operators

In FEEC, we have canonical prolongation and restriction operators for a hierarchy of meshes. In the case of DEC, we can exploit this to get restriction and prolongation operators for cochains on different meshes.

Let $\mathring{V}_k^{h,\ell}$ denote the space of Whitney k-forms on the ℓ-times regularly refined initial mesh $\mathcal{T}$, denoted by $\mathcal{T}_\ell$, and let $\tilde{P}_{\ell,\ell+1}^k$ denote the canonical prolongation operator of the Whitney forms from $\mathring{V}_k^{h,\ell}$ to $\mathring{V}_k^{h,\ell+1}$. We define the prolongation operator for DEC by

$$P_{\ell,\ell+1}^k := \mathcal{R}_{h,\ell+1}^k \tilde{P}_{\ell,\ell+1}^k \mathcal{W}_{h,\ell}^k,$$

where the subscript "h,ℓ" for $\mathcal{R}$ and $\mathcal{W}$ denotes the corresponding operator on the ℓ-times refined mesh, i.e. we go from chochains on $\mathcal{T}_\ell^k$ to Whitney forms via $\mathcal{W}_{h,\ell}^k$, prolong there and then go to cochains on $\mathcal{T}_{\ell+1}^k$ via the de Rham map $\mathcal{R}_{h,\ell+1}^k$. In terms of matrices, as mentioned before, $\mathcal{R}_{\bullet,\bullet}^{\bullet}$ and $\mathcal{W}_{\bullet,\bullet}^{\bullet}$ are represented by identity matrices on the respective spaces if standard bases are used, so the FEEC and DEC prolongation matrices coincide. We can extend the prolongation to $\mathring{C}(\mathcal{T})$ by defining it as $P_{\ell,\ell+1} := \bigoplus P_{\ell,\ell+1}^k$.

For the restriction operator, we cannot just take the transpose, as $\mathrm{D}^{\mathrm{DEC}}$ does not arise from a finite element discretization. Instead, we look at $A_{h,\ell+1}^{\mathrm{DEC}} := \mathrm{M}_{h,\ell+1}^{\mathrm{DEC}} \mathrm{D}_{\ell+1}^{\mathrm{DEC}}$, where $\mathrm{M}_{h,\ell+1}^{\mathrm{DEC}}$ denotes the DEC mass matrix and $\mathrm{D}_{\ell+1}^{\mathrm{DEC}}$ the DEC Dirac operator at the level ℓ, which is a mass-lumped FEEC matrix as was explained in Remark 3.12. We multiply the problem from (3.12) by $\mathrm{M}^{\mathrm{DEC}}$ and regard it as a finite element equation, that is, given the problem

$$\mathrm{D}_{\ell+1}^{\mathrm{DEC}} \mathbf{u} = \mathbf{f},$$

we look for a coarse grid correction for solving

$$A_{h,\ell+1}^{\mathrm{DEC}} \mathbf{u} = \mathrm{M}_{h,\ell+1}^{\mathrm{DEC}} \mathrm{D}_{\ell+1}^{\mathrm{DEC}} \mathbf{u} = \mathrm{M}_{h,\ell+1}^{\mathrm{DEC}} \mathbf{f}.$$

The coarse grid correction is given by

$$\begin{aligned} \mathbf{u} \mapsto & \mathbf{u} + P_{\ell,\ell+1} \left(A_{h,\ell}^{\mathrm{DEC}} \right)^{-1} P_{\ell,\ell+1}^T \left(\mathrm{M}_{h,\ell+1}^{\mathrm{DEC}} \mathbf{f} - A_{h,\ell+1}^{\mathrm{DEC}} \mathbf{u} \right) \\ = & \mathbf{u} + P_{\ell,\ell+1} \left(\mathrm{D}_{\ell}^{\mathrm{DEC}} \right)^{-1} \left[\left(\mathrm{M}_{h,\ell}^{\mathrm{DEC}} \right)^{-1} P_{\ell,\ell+1}^T \mathrm{M}_{h,\ell+1}^{\mathrm{DEC}} \right] \left(\mathbf{f} - \mathrm{D}_{\ell+1}^{\mathrm{DEC}} \mathbf{u} \right). \end{aligned}$$

The obvious choice for the restriction operator for solving $\mathrm{D}^{\mathrm{DEC}}_{\ell+1}\mathbf{u} = \mathbf{f}$ is then

$$R_{\ell+1,\ell} := \left(\mathrm{M}^{\mathrm{DEC}}_{h,\ell}\right)^{-1} P^T_{\ell,\ell+1}\mathrm{M}^{\mathrm{DEC}}_{h,\ell+1}.$$

As can be seen, this is the adjoint of the prolongation operator, but w.r.t. the DEC inner product as opposed to the standard inner product on vectors.

3.4.2 Distributive Relaxation

In the context of DEC we can quite easily define a transforming smoother in the sense of Section 2.4.1. If we want to solve a linear system of equations of the form

$$\mathrm{D}^{\mathrm{DEC}}\mathbf{u} = \mathbf{f},$$

where $\mathbf{f} \in \operatorname{ran}\mathrm{D}^{\mathrm{DEC}}$, we can do the same as in the structured case and construct a transforming smoother using the block-diagonal DEC Hodge-Laplacian

$$\left(\mathrm{D}^{\mathrm{DEC}}\right)^2 = \begin{pmatrix} \delta^{\mathrm{DEC}}_1\partial_0 & & & & & \\ & \partial^0\delta^{\mathrm{DEC}}_1 + \delta^{\mathrm{DEC}}_2\partial^1 & & & & \\ & & \ddots & & & \\ & & & \partial^{k-1}\delta^{\mathrm{DEC}}_k + \delta^{\mathrm{DEC}}_{k+1}\partial^k & & \\ & & & & \ddots & \\ & & & & & \partial^{n-1}\delta^{\mathrm{DEC}}_n \end{pmatrix},$$

where we used $\partial^{k+1}\partial^k \equiv 0$ and $\delta^{\mathrm{DEC}}_k\delta^{\mathrm{DEC}}_{k+1} \equiv 0$[2].

We can define a DGSR of the form

DGSR on Unstructured Grids

$$\mathbf{u} \mapsto \mathbf{u} + \mathrm{D}^{\mathrm{DEC}}\left(\operatorname{tril}\left(\mathrm{D}^{\mathrm{DEC}}\right)^2\right)^{-1}\left(\mathbf{f} - \mathrm{D}^{\mathrm{DEC}}\mathbf{u}\right).$$

Of course it is highly desirable for $\mathrm{D}^{\mathrm{DEC}}$ to only perform local operations, which is given if we use the Hodge star from Definition 3.6.

Remark 3.30 *In complete analogy to Remark 2.3, we can define an l-transforming smoother*

$$\mathbf{u} \mapsto \mathbf{u} + \left(\operatorname{tril}\left(\mathrm{D}^{\mathrm{DEC}}\right)^2\right)^{-1}\mathrm{D}^{\mathrm{DEC}}\left(\mathbf{f} - \mathrm{D}^{\mathrm{DEC}}\mathbf{u}\right),$$

which is again analogous to solving the squared system with an appropriate right-hand-side.

Note that unlike in the structured case, $\left(\mathrm{D}^{\mathrm{DEC}}\right)^2$ is no longer symmetric, so the proof of convergence from Proposition 2.4 cannot be applied here. Nonetheless, one can show that the iteration still converges as can be seen from the proposition below.

[2]Assume that the boundary values have already been eliminated, that is, the respective rows and columns set to zero and filled with ones on the diagonal. Alternatively, one can delete the respective rows and columns and remove the entries from the load and solution vector.

Proposition 3.31
Let $\left(\mathrm{D}^{\mathrm{DEC}}\right)^2 = L + D + U, M := L + D = \mathrm{tril}\left(\mathrm{D}^{\mathrm{DEC}}\right)^2$*, where* L *denotes the lower triangular,* U *the upper triangular and* D *the diagonal part of* $\left(\mathrm{D}^{\mathrm{DEC}}\right)^2$ *and define the error propagation matrix* $E := 1 - \mathrm{D}^{\mathrm{DEC}} M^{-1} \mathrm{D}^{\mathrm{DEC}}$*, then*

$$\forall x \in \left(\ker \mathrm{D}^{\mathrm{DEC}}\right)^{\perp_{\mathrm{DEC}}} \setminus \{0\} : |||Ex||| < |||x|||.$$

Proof The proof is mostly the same as in Proposition 2.4.

For any $x \in \mathring{C}(\mathcal{T})$, we have

$$\begin{aligned}
[\![Ex, Ex]\!] &= [\![x, x]\!] - \left[\!\left[x, \mathrm{D}^{\mathrm{DEC}} M^{-1} \mathrm{D}^{\mathrm{DEC}} x\right]\!\right] - \left[\!\left[\mathrm{D}^{\mathrm{DEC}} M^{-1} \mathrm{D}^{\mathrm{DEC}} x, x\right]\!\right] \\
&\quad + \left[\!\left[\mathrm{D}^{\mathrm{DEC}} M^{-1} \mathrm{D}^{\mathrm{DEC}} x, \mathrm{D}^{\mathrm{DEC}} M^{-1} \mathrm{D}^{\mathrm{DEC}} x\right]\!\right] \\
&= [\![x, x]\!] - \left[\!\left[\mathrm{D}^{\mathrm{DEC}} x, M^{-1} \mathrm{D}^{\mathrm{DEC}} x\right]\!\right] - \left[\!\left[M^{-1} \mathrm{D}^{\mathrm{DEC}} x, \mathrm{D}^{\mathrm{DEC}} x\right]\!\right] \\
&\quad + \left[\!\left[\mathrm{D}^{\mathrm{DEC}} M^{-1} \mathrm{D}^{\mathrm{DEC}} x, \mathrm{D}^{\mathrm{DEC}} M^{-1} \mathrm{D}^{\mathrm{DEC}} x\right]\!\right],
\end{aligned}$$

as $\mathrm{D}^{\mathrm{DEC}}$ is self-adjoint.

Now make the substitution $z := M^{-1} \mathrm{D}^{\mathrm{DEC}} x \iff Mz = \mathrm{D}^{\mathrm{DEC}} x$. Then

$$[\![Ex, Ex]\!] = [\![x, x]\!] - [\![Mz, z]\!] - [\![z, Mz]\!] + \left[\!\left[\mathrm{D}^{\mathrm{DEC}} z, \mathrm{D}^{\mathrm{DEC}} z\right]\!\right].$$

What is left to prove is

$$\left[\!\left[\mathrm{D}^{\mathrm{DEC}} z, \mathrm{D}^{\mathrm{DEC}} z\right]\!\right] < [\![Mz, z]\!] + [\![z, Mz]\!].$$

Recall that for any $a, b \in \mathring{C}(\mathcal{T})$, we have

$$[\![a, b]\!] = \vec{a}^T \mathrm{M}^{\mathrm{DEC}} \vec{b},$$

where $\vec{a}, \vec{b}$ are the coefficient vectors of a, b and $\mathrm{M}^{\mathrm{DEC}}$ is the *diagonal* DEC mass matrix. It follows that

$$[\![z, Mz]\!] = \left[\!\left[\left(\mathrm{M}^{\mathrm{DEC}}\right)^{-1} M^T \mathrm{M}^{\mathrm{DEC}} z, z\right]\!\right].$$

$\mathrm{M}^{\mathrm{DEC}} \mathrm{D}^{\mathrm{DEC}}$ is self-adjoint w.r.t. the usual inner product, i.e. symmetric, hence

$$\begin{aligned}
&\mathrm{M}^{\mathrm{DEC}} \mathrm{D}^{\mathrm{DEC}} = \left(\mathrm{M}^{\mathrm{DEC}} \mathrm{D}^{\mathrm{DEC}}\right)^T = \left(\mathrm{D}^{\mathrm{DEC}}\right)^T \mathrm{M}^{\mathrm{DEC}} \\
\iff &\mathrm{D}^{\mathrm{DEC}} = \left(\mathrm{M}^{\mathrm{DEC}}\right)^{-1} \left(\mathrm{D}^{\mathrm{DEC}}\right)^T \mathrm{M}^{\mathrm{DEC}} \\
\implies &\left(\mathrm{D}^{\mathrm{DEC}}\right)^2 = \left(\mathrm{M}^{\mathrm{DEC}}\right)^{-1} \left[\left(\mathrm{D}^{\mathrm{DEC}}\right)^2\right]^T \mathrm{M}^{\mathrm{DEC}} \\
\iff &L + D + U = \left(\mathrm{M}^{\mathrm{DEC}}\right)^{-1} (L^T + D + U^T) \mathrm{M}^{\mathrm{DEC}}.
\end{aligned}$$

By comparing the upper triagonal parts of the above ($\mathrm{M}^{\mathrm{DEC}}$ is diagonal), it must hold that

$$U = \left(\mathrm{M}^{\mathrm{DEC}}\right)^{-1} L^T \mathrm{M}^{\mathrm{DEC}}.$$

Finally, we get

$$\begin{aligned}
[\![Mz, z]\!] + [\![z, Mz]\!] &= \left[\!\!\left[\left(L + D + \left(\mathrm{M}^{\mathrm{DEC}}\right)^{-1} (L^T + D)\mathrm{M}^{\mathrm{DEC}} \right) z, z \right]\!\!\right] \\
&= [\![((D + L) + (D + U))\, z, z]\!] \\
&= \left[\!\!\left[\left(\left(\mathrm{D}^{\mathrm{DEC}}\right)^2 + D \right) z, z \right]\!\!\right] \\
&= \left[\!\!\left[\mathrm{D}^{\mathrm{DEC}} z, \mathrm{D}^{\mathrm{DEC}} z \right]\!\!\right] + [\![Dz, z]\!] \\
&> \left[\!\!\left[\mathrm{D}^{\mathrm{DEC}} z, \mathrm{D}^{\mathrm{DEC}} z \right]\!\!\right],
\end{aligned}$$

as we know that $D > 0$ and that $z \neq 0$ by the assumption of the lemma: $0 \neq x \in \left(\ker \mathrm{D}^{\mathrm{DEC}}\right)^{\perp_{\mathrm{DEC}}} \implies z = M^{-1}\mathrm{D}^{\mathrm{DEC}} x \neq 0$. □

As in Proposition 2.4, the algorithm only eliminates error components in $\left(\ker \mathrm{D}^{\mathrm{DEC}}\right)^{\perp_{\mathrm{DEC}}}$ and stays in $\operatorname{ran} \mathrm{D}^{\mathrm{DEC}}$ if the start vector is in $\operatorname{ran} \mathrm{D}^{\mathrm{DEC}}$, i.e. it preserves the components in the harmonic forms and eliminates the other ones.

Remark 3.32 *Note that the prolongation of an element in $\mathring{C}(\mathcal{T}_\ell)$ is mapped to $\mathring{C}(\mathcal{T}_{\ell+1})$, that is, the trivial harmonic forms are preserved. If we had considered a problem with non-trivial topology, it is not clear why the transfer operators should preserve orthogonality, i.e.*

$$P_{\ell,\ell+1} \left(\ker \mathrm{D}_\ell^{\mathrm{DEC}}\right)^{\perp_{\mathrm{DEC}}} \subset \left(\ker \mathrm{D}_{\ell+1}^{\mathrm{DEC}}\right)^{\perp_{\mathrm{DEC}}}$$

and the corresponding relation for the restriction operator might not be fulfilled.

As distributive relaxation only eliminates components which are in $\left(\ker \mathrm{D}^{\mathrm{DEC}}\right)^{\perp}$, if the transfer operators incur an error component in the harmonic forms, these will never be eliminated by the multigrid solver.

Using the l-transforming smoother from Remark 3.30 does not solve this issue, or rather, it could actively incur error components in the harmonic forms as it is not clear why the added correction should be in $\operatorname{ran} \mathrm{D}^{\mathrm{DEC}}$.

The exploration of harmonic forms exceeds the scope of this thesis. However, it remains an intriguing subject for further investigation.

3.4.3 Smoother for FEEC

As we know that by Theorem 3.20 A^{DEC} and A^{FEEC} are spectrally equivalent, we can attempt to construct a smoother for the FEEC problem from the one applied to the problem arising from $A^{\mathrm{DEC}} \equiv \mathrm{M}^{\mathrm{DEC}}\mathrm{D}^{\mathrm{DEC}}$. The r-transforming smoother for $A^{\mathrm{DEC}}\mathbf{u} = \mathbf{f}$ using the r-transformation $\mathrm{D}^{\mathrm{DEC}}$ yields a smoother

$$\mathbf{u} \mapsto \mathbf{u} + \mathrm{D}^{\mathrm{DEC}} \left(\operatorname{tril} \mathrm{M}^{\mathrm{DEC}} \left(\mathrm{D}^{\mathrm{DEC}}\right)^2 \right)^{-1} \left(\mathbf{f} - A^{\mathrm{DEC}}\mathbf{u} \right).$$

Note that $A^{\mathrm{DEC}}\mathrm{D}^{\mathrm{DEC}} = \mathrm{M}^{\mathrm{DEC}} \left(\mathrm{D}^{\mathrm{DEC}}\right)^2$ is block-diagonal and symmetric due to the fact that $\left(\mathrm{D}^{\mathrm{DEC}}\right)^2$ is self-adjoint w.r.t. the DEC inner product.

Replacing the residual by the one of the spectrally equivalent FEEC problem $A^{\mathrm{FEEC}} u_h = f_h$[3] yields the smoother

DEC-Based DGSR for FEEC

$$u_h \mapsto u_h + \mathrm{D}^{\mathrm{DEC}} \left(\operatorname{tril} \mathrm{M}^{\mathrm{DEC}} \left(\mathrm{D}^{\mathrm{DEC}} \right)^2 \right)^{-1} \left(f_h - A^{\mathrm{FEEC}} u_h \right). \tag{3.18}$$

3.5 Numerical Results

The multigrid algorithm described in this chapter was implemented using `MFEM`, see [1]. The code is available at https://gitlab.ethz.ch/rdabetic/master-thesis.

3.5.1 Two Dimensions

We employ the method of manufactured solutions to empirically verify the order of convergence obtained in Proposition 3.28. We measure DEC norms of the discretization error $e := \mathcal{R}\mathfrak{u} - \mathbf{u}$, $\mathbf{u}$ solution of (3.12), where $\mathcal{R}\mathfrak{u}$ and $\mathcal{R}\mathfrak{f}$ are computed by "overkill quadrature", which means that the quadrature error is negligible compared to the discretization error. We monitor two error norms: When we talk about the DEC L^2-norm we mean $|||e|||$, and by the DEC $H\Lambda$-norm we mean $|||e||| + \left|\left|\left| \mathrm{d}^{\mathrm{DEC}} e \right|\right|\right|$.

We also tested the convergence rates of a V-cycle by performing a power iteration.

Test I

We consider the unit square $\Omega = [0,1]^2$ and fix the right-hand-side $\mathfrak{f}$ such that we obtain a smooth solution of (1.7), which reads

$$u_0 = \sin 2\pi x \sin 2\pi y, \quad u_1 = (\sin 2\pi y, \sin 2\pi x)^T, \quad u_2 = \cos 2\pi x \sin 2\pi y$$

in Euclidean vector proxies.

The coarsest mesh that was used is displayed in Figure 3.1a. It was refined several times using regular refinement, i.e. connecting the midpoints of the edges to split each triangle into four smaller ones.

The resulting error norms are plotted in Figure 3.1b, and we observe first-order convergence, exactly the order of convergence predicted by Proposition 3.28.

The multigrid convergence rates can be found in Table 3.1a, and it can be seen that the method displays mesh-width independent convergence.

Test II

Similar to [12], we tested the DEC discretization on a triangle as well. As a domain $\Omega \subset \mathbb{R}^2$ we chose an equilateral triangle with vertices at $(0,0)$, $(0,1)$, and $\left(1/2, \sqrt{3}/2\right)$. We fix the right-hand-side such that we obtain the exact solution (in Euclidean vector proxies)

$$u_0 = 2^{15} \left(\lambda_0 \lambda_1 \lambda_2\right)^3, \quad u_1 = (u_0, u_0)^T, \quad u_2 = u_0 - \frac{1}{|\Omega|} \int_\Omega u_0(x,y) \, \mathrm{d}x\mathrm{d}y,$$

where λ_i denotes the barycentric coordinate function associated with vertex i.

[3] We re-interpret $\mathbf{u}, \mathbf{f}$ as u_h, f_h via the Whitney isomorphism.

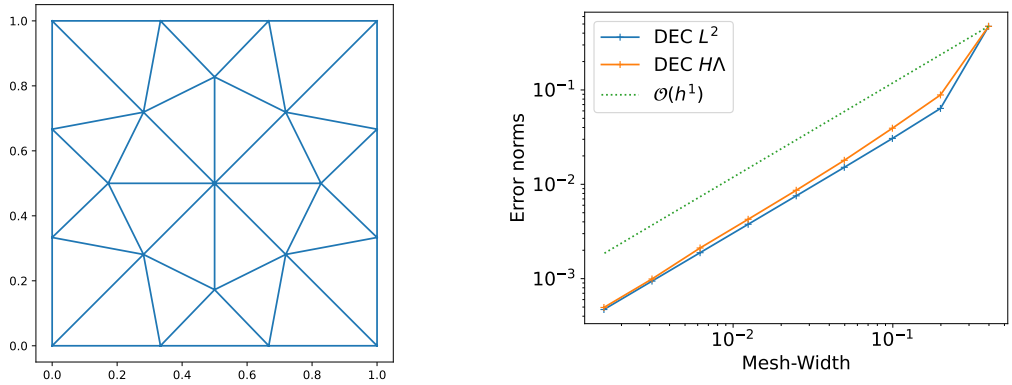

(a) Test I: Coarsest mesh

(b) Test I: Error norms

Figure 3.1: Mesh and convergence of DEC on a square.

As before, we used successive regular refinement of a coarse mesh, which can be seen in Figure 3.2a, to generate a sequence of meshes with decreasing mesh-width. Note that the refined meshes only contain equilateral triangles.

The plot of Figure 3.2b clearly reveals that for $h \to 0$ the error norms decrease faster than expected. The better-than-expected order of convergence is most likely due to the symmetry of the mesh (all equilateral triangles), as explained in [12, Section 6], where the authors provide improved error estimates on $\mathcal{R} - J$ in such a case. Concretely, [12, Equation 6.2 & Proposition 6.2] establish second order convergence, which is what is observed. For the multigrid convergence, see Table 3.1b, where we see that it works

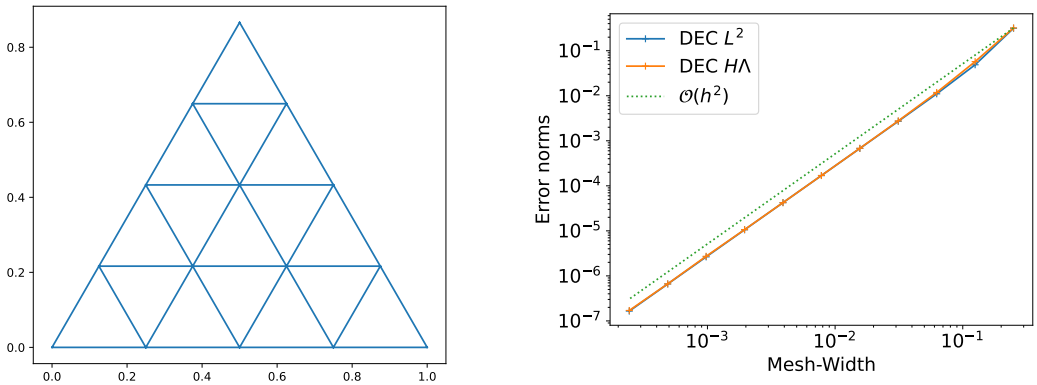

(a) Test II: Coarsest mesh

(b) Test II: Error norms

Figure 3.2: Mesh and convergence of DEC on an equilateral triangle with a structured mesh.

as anticipated.

Test III

This numerical experiment is inspired by the "Perturbed Mesh" computation in [12, Section 7]. The setup is the same as in Test II, but now we start with a slightly perturbed coarse mesh of the triangle domain Ω, see Figure 3.3a. This breaks symmetries, the theory from [12, Section 6] no longer applies and, as one can see from Figure 3.3b, now convergence of error norms appears to be first order, albeit with some pre-asymptotic behavior.

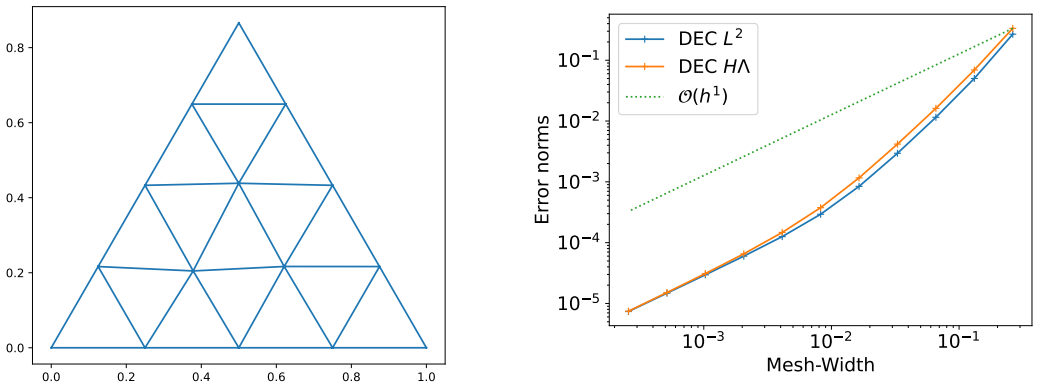

(a) Test III: Coarsest mesh

(b) Test III: Error norms

Figure 3.3: Mesh and convergence of DEC on an equilateral triangle with a perturbed mesh.

For the multigrid convergence, see Table 3.1c, where we see that while being robust, the convergence rate has decreased compared to the unperturbed case.

Level	h	$\lvert\lambda_{\max}\rvert$
1	1.99E-01	4.53E-01
2	9.94E-02	7.71E-01
3	4.97E-02	7.92E-01
4	2.48E-02	8.01E-01
5	1.24E-02	8.09E-01
6	6.21E-03	8.15E-01
7	3.11E-03	8.15E-01
8	1.55E-03	8.17E-01

(a) Square

Level	h	$\lvert\lambda_{\max}\rvert$
1	1.25E-01	1.88E-01
2	6.25E-02	2.49E-01
3	3.12E-02	2.69E-01
4	1.56E-02	2.76E-01
5	7.81E-03	2.87E-01
6	3.91E-03	3.02E-01
7	1.95E-03	3.08E-01
8	9.77E-04	3.15E-01

(b) Triangle with a regular mesh

Level	h	$\lvert\lambda_{\max}\rvert$
1	1.37E-01	1.78E-01
2	6.84E-02	3.81E-01
3	3.42E-02	4.50E-01
4	1.71E-02	2.78E-01
5	8.56E-03	5.01E-01
6	4.28E-03	5.08E-01
7	2.14E-03	5.14E-01
8	1.07E-03	5.11E-01

(c) Triangle with a perturbed mesh

Table 3.1: DEC multigrid convergence rates on different meshes in 2D (with circumcentric duals). The mesh-width is denoted by h.

Test IV

In this test, a coarse mesh of $\Omega = [0,1]^2 \setminus [1/4, 3/4]^2$, a domain with a non-trivial topology, see Figure 3.4, was used to investigate the convergence of just the multigrid method.

To solve the linear system at the coarsest level, a sparse QR factorization was used to

compute the least-squares solution.

The domain in Figure 3.4 has exactly one hole and connected component, hence we expect the dimension of the space of non-trivial harmonic forms to be equal to one, that is, the sum off all Betti numbers minus one (we exclude the trivial ones). Thus, by applying our theoretical understanding gained in Remark 3.32, we conjecture that the error matrix of a V-cycle will display exactly one eigenvalue of magnitude one.

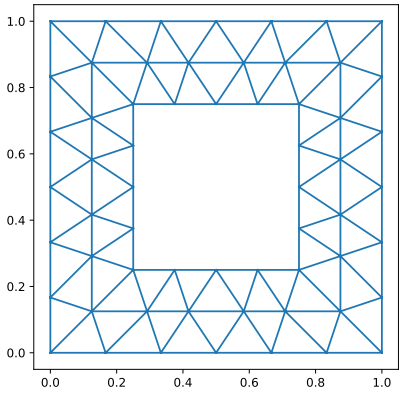

Figure 3.4: Test IV: Coarsest Mesh

Level	h	$\lvert\lambda_0\rvert$	$\lvert\lambda_1\rvert$	$\lvert\lambda_2\rvert$
1	8.838835E-02	9.999992E-01	3.261091E-01	3.017770E-01
2	4.419417E-02	9.999919E-01	4.413730E-01	4.418638E-01
3	2.209709E-02	9.999844E-01	4.917262E-01	4.918557E-01
4	1.104854E-02	9.999879E-01	5.095853E-01	5.089627E-01
5	5.524272E-03	9.999819E-01	5.151095E-01	5.183340E-01

Table 3.2: Test IV: Absolute value of the (approximate) largest three eigenvalues of the error matrix of a V-cycle on Figure 3.4.

By using a power iteration with deflation, that is, seeking an eigenvector in the orthogonal complement of the ones already computed, the largest (in magnitude) few eigenvalues were approximated. The results are recorded in Table 3.2.

As can be observed in Table 3.2, exactly one eigenvalue with magnitude one (up to rounding errors) appears to manifest itself, reinforcing the understanding presented in Remark 3.32.

Test V

To further investigate how the dimension of the space of harmonic forms influences convergence, a test was carried out on the domain found in Figure 3.5, which is anticipated to give rise to *two* non-trivial harmonic forms, in contrast to *one* in test IV. Therefore we may expect to find two eigenvalues of magnitude one.

The results can be found in Table 3.3 and as can be seen, two harmonic forms produce two eigenvalues of unit magnitude.

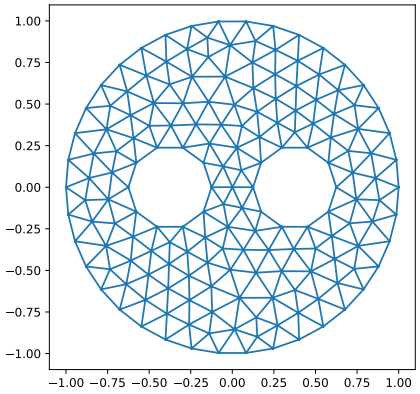

Figure 3.5: Test V: Coarsest Mesh

Level	h	$\lvert\lambda_0\rvert$	$\lvert\lambda_1\rvert$	$\lvert\lambda_2\rvert$
1	9.961539E-02	9.999961E-01	9.999992E-01	3.236872E-01
2	4.980769E-02	1.000066E+00	9.999767E-01	8.240601E-01
3	2.490385E-02	1.000092E+00	9.998758E-01	8.446312E-01
4	1.245192E-02	9.999391E-01	9.999369E-01	8.596365E-01
5	6.225962E-03	9.999812E-01	9.998069E-01	8.612764E-01

Table 3.3: Test V: Absolute value of the (approximate) largest three eigenvalues of the error matrix of a V-cycle on Figure 3.5.

3.5.2 Three Dimensions

We were unable to find suitable meshes to test the convergence of DEC, so we used dual meshes based on the *barycenters* to test the convergence of the multigrid method[4]. Even if we have a well-centered coarse mesh, the refinement techniques used in `MFEM` do not have to preserve well-centeredness in 3D, meaning it may not be trivial to generate a hierarchy of well-centered meshes. Regarding well-centered meshing in 3D, there appears to have been some research, see [25], which we shall not dwell on as it is not the main topic of this thesis.

The convergence of a V-cycle was tested on three different meshes: a mesh of the unit cube $[0,1]^3$, a coarse mesh of a unit ball and a regular tetrahedron with vertices at $(-1/2, 0, 0)$, $(1/2, 0, 0)$, $\left(0, \sqrt{3}/2, 0\right)$, $\left(0, \sqrt{3}/6, \sqrt{2/3}\right)$. The corresponding convergence rates can be found in Table 3.4a, Table 3.4b and Table 3.4c respectively. The method displays convergence rates which are independent of the mesh-width.

3.5.3 FEEC

To test whether the smoother from (3.18) works as intended, as we did not provide any theoretical results, we tested the convergence of the multigrid algorithm for the FEEC problem in 2D on the same meshes as in the DEC case (see Section 3.5.1), but now with *barycentric* duals.

The results for meshes with trivial topologies can be found in Table 3.5, and as can be seen, we observe robust convergence rates across all the problems.

For problems with a non-trivial topology, refer to Table 3.6.

[4]The dual mesh was obtained by connecting the barycenters of a k-simplex to the barycenters of the $(k-1)$-simplices which are a part of the k-simplex. This leads to a non-orthogonal dual mesh (with kinks).

Level	h	$\lvert\lambda_{\max}\rvert$
1	4.13E-01	6.65E-01
2	2.06E-01	6.95E-01
3	1.03E-01	7.00E-01
4	5.16E-02	6.81E-01
5	2.58E-02	6.87E-01

(a) Cube

Level	h	$\lvert\lambda_{\max}\rvert$
1	3.25E-01	6.93E-01
2	1.62E-01	7.07E-01
3	8.11E-02	7.12E-01
4	4.06E-02	7.18E-01
5	2.03E-02	7.15E-01

(b) Coarse Mesh of a Ball

Level	h	$\lvert\lambda_{\max}\rvert$
1	7.07E-01	5.67E-01
2	3.54E-01	6.03E-01
3	1.77E-01	5.77E-01
4	8.84E-02	5.84E-01
5	4.42E-02	5.84E-01

(c) Regular Tetrahedron

Table 3.4: DEC Multigrid convergence rates on different meshes in 3D. The mesh-width is denoted by h.

Level	h	$\lvert\lambda_{\max}\rvert$
1	1.99E-01	3.07E-01
2	9.94E-02	3.83E-01
3	4.97E-02	4.20E-01
4	2.48E-02	4.51E-01
5	1.24E-02	4.65E-01
6	6.21E-03	4.71E-01
7	3.11E-03	4.75E-01
8	1.55E-03	4.76E-01

(a) Square

Level	h	$\lvert\lambda_{\max}\rvert$
1	1.25E-01	2.45E-01
2	6.25E-02	2.61E-01
3	3.12E-02	2.63E-01
4	1.56E-02	2.91E-01
5	7.81E-03	2.92E-01
6	3.91E-03	2.60E-01
7	1.95E-03	3.07E-01
8	9.77E-04	3.14E-01

(b) Triangle with a regular mesh

Level	h	$\lvert\lambda_{\max}\rvert$
1	1.32E-01	2.07E-01
2	6.58E-02	2.60E-01
3	3.29E-02	2.82E-01
4	1.65E-02	2.94E-01
5	8.23E-03	3.23E-01
6	4.11E-03	3.35E-01
7	2.06E-03	3.46E-01
8	1.03E-03	3.50E-01

(c) Triangle with a perturbed mesh

Table 3.5: FEEC Multigrid convergence rates on different meshes in 2D (with barycentric duals). The mesh-width is denoted by h.

Level	h	$\lvert\lambda_0\rvert$	$\lvert\lambda_1\rvert$	$\lvert\lambda_2\rvert$
1	8.838835E-02	9.999992E-01	2.921614E-01	2.845712E-01
2	4.419417E-02	9.999814E-01	4.094331E-01	4.091378E-01
3	2.209709E-02	9.999942E-01	4.541379E-01	4.534524E-01
4	1.104854E-02	9.999925E-01	4.700092E-01	4.690883E-01
5	5.524272E-03	9.999803E-01	4.773131E-01	4.781302E-01

(a) Absolute value of the (approximate) largest three eigenvalues of the error matrix of a V-cycle for FEEC on Figure 3.4.

Level	h	$\lvert\lambda_0\rvert$	$\lvert\lambda_1\rvert$	$\lvert\lambda_2\rvert$
1	9.961539E-02	9.999978E-01	9.999957E-01	3.161215E-01
2	4.980769E-02	9.999931E-01	9.999950E-01	3.630346E-01
3	2.490385E-02	9.999927E-01	9.999884E-01	3.999449E-01
4	1.245192E-02	9.999834E-01	9.999896E-01	4.561642E-01
5	6.225962E-03	9.999909E-01	9.999799E-01	4.713637E-01

(b) Absolute value of the (approximate) largest three eigenvalues of the error matrix of a V-cycle for FEEC on Figure 3.5.

Table 3.6: FEEC Multigrid convergence rates on different meshes in 2D (with barycentric duals) with non-trivial topology. The mesh-width is denoted by h.

It appears to behave exactly the same as DEC in regards to the number of eigenvalues with unit magnitude, which comes as no surprise as we expect the dimension of the space of harmonic forms to be the same.

Chapter 4

Conclusion

In conclusion, this thesis successfully developed methodologies for solving the boundary value problem associated with the Hodge-Dirac operator within a bounded, Lipschitz, polytopal, and *topologically trivial* domain $\Omega \subset \mathbb{R}^n$. Using a geometric multigrid method, we effectively solved the system of linear equations derived from DEC and FEEC discretizations.

We first confirmed the persistence of the "Dirac$^2 = -\Delta$" property in the discrete context with mass-lumped FEEC on structured grids using explicit computation by hand and used the insight gained to design a smoother for a multigrid method in both 2D and 3D, which was validated numerically.

We saw that the property "Dirac$^2 = -\Delta$" extends to the unstructured case in the DEC-setting and extended the smoother from the structured case to the unstructured case. A multigrid method for solving the boundary value problem in the context of DEC was elucidated and tested successfully.

We proved that under the assumption of h-uniform norm equivalence, i.e. Assumption 3.3.1, we have a Poincaré inequality for DEC, which we used to prove stability of DEC based on [19], culminating in a proof of the spectral equivalence between FEEC and DEC. In addition, a smoother for the FEEC problem based on the DEC problem was proposed and tested in 2D, showing promising results.

Furthermore, we proved and verified the convergence of DEC under the assumption of a well-centered mesh with circumcentric duals using techniques established in [12].

Future directions include investigating the smoothers (especially the FEEC smoother) more closely, as well as exploring ways of dealing with non-trivial topologies and the non-trivial harmonic forms arising therefrom, e.g. by combining the multigrid method with an iterative solver. Additionally, it would be interesting to see whether the techniques in this thesis, i.e. using DEC to build a transforming smoother, can be applied to other problems.

Appendix A

3D Matrices

A.1 Local DOF and Element Matrix

Let $\hat{\mathbf{i}}, \hat{\mathbf{j}}, \hat{\mathbf{k}}$ be the unit vectors in x, y, z respectively, then the local DOF on the reference element with the ordering from Figure 2.10 are given by (see [23])

- u_0 :

$$\begin{aligned} -\mathbf{xyz} + \mathbf{xy} + \mathbf{xz} - \mathbf{x} + \mathbf{yz} - \mathbf{y} - \mathbf{z} + 1, \\ \mathbf{x}\left(\mathbf{yz} - \mathbf{y} - \mathbf{z} + 1\right), \\ \mathbf{y}\left(\mathbf{xz} - \mathbf{x} - \mathbf{z} + 1\right), \\ \mathbf{xy}\left(1 - \mathbf{z}\right), \\ \mathbf{z}\left(\mathbf{xy} - \mathbf{x} - \mathbf{y} + 1\right), \\ \mathbf{xz}\left(1 - \mathbf{y}\right), \\ \mathbf{yz}\left(1 - \mathbf{x}\right), \\ \mathbf{xyz} \end{aligned}$$

- $\mathbf{u}_1$:

$$\begin{aligned} \left(\mathbf{yz} - \mathbf{y} - \mathbf{z} + 1\right)\hat{\mathbf{i}}, \\ \left(\mathbf{xz} - \mathbf{x} - \mathbf{z} + 1\right)\hat{\mathbf{j}}, \\ \left(\mathbf{xy} - \mathbf{x} - \mathbf{y} + 1\right)\hat{\mathbf{k}}, \\ \left(\mathbf{x}\left(1 - \mathbf{z}\right)\right)\hat{\mathbf{j}}, \\ \left(\mathbf{x}\left(1 - \mathbf{y}\right)\right)\hat{\mathbf{k}}, \\ \left(\mathbf{y}\left(1 - \mathbf{z}\right)\right)\hat{\mathbf{i}}, \\ \left(\mathbf{y}\left(1 - \mathbf{x}\right)\right)\hat{\mathbf{k}}, \\ \left(\mathbf{xy}\right)\hat{\mathbf{k}}, \\ \left(\mathbf{z}\left(1 - \mathbf{y}\right)\right)\hat{\mathbf{i}}, \\ \left(\mathbf{z}\left(1 - \mathbf{x}\right)\right)\hat{\mathbf{j}}, \\ \left(\mathbf{xz}\right)\hat{\mathbf{j}}, \\ \left(\mathbf{yz}\right)\hat{\mathbf{i}} \end{aligned}$$

- $\mathbf{u_2}$:

$$\left(1 - \mathbf{z}\right)\hat{\mathbf{k}},\ \left(1 - \mathbf{y}\right)\hat{\mathbf{j}},\ \left(1 - \mathbf{x}\right)\hat{\mathbf{i}},\ \left(\mathbf{x}\right)\hat{\mathbf{i}},\ \left(\mathbf{y}\right)\hat{\mathbf{j}},\ \left(\mathbf{z}\right)\hat{\mathbf{k}}$$

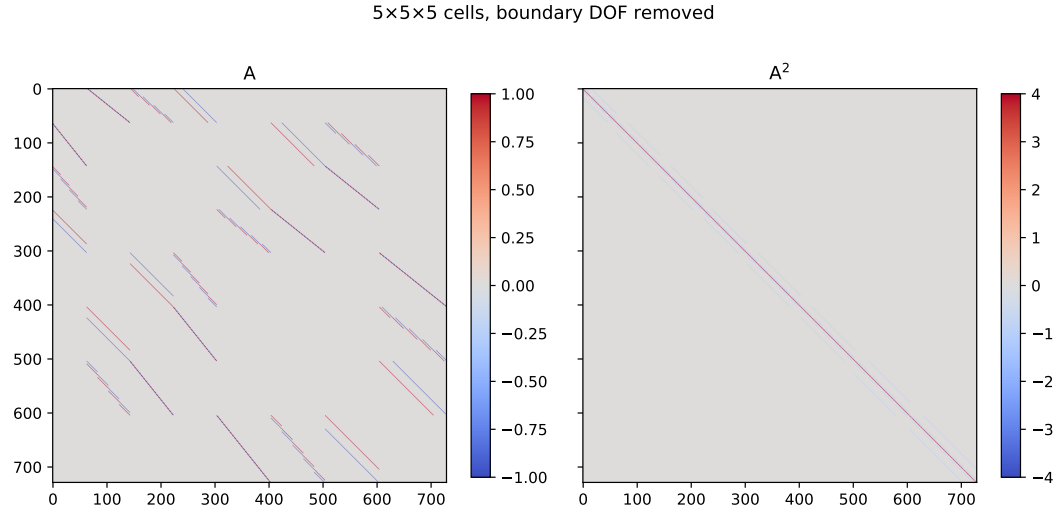

Figure A.1: Fully assembled 3D Galerkin matrix with the boundary DOF dropped with 5^3 cells multiplied by $\frac{1}{h^2}$, so all entries are in units of h^2, and its square.

- $u_3 : 1$.

The local element matrix on the reference element is given by Table A.1.

A.2 Stencils

In order to verify that we indeed get back the 7-point stencils for $-\Delta$ in 3D as well, one can assemble a small grid and look at the rows corresponding to the interior DOF. We chose a grid with 5^3 cells, with the enumeration of the DOF of the 6-dimensional vector in the order of the vector components and then the x_1, x_2 and x_3 direction. The Galerkin matrix (with normalized entries) can be found in Figure A.1. The script also extracts a row of A_h^2 corresponding to an interior DOF, the output of which is:

```
    --- N = 5 ---
Non-Zero locations and entries in an interior vertex-row:
    [ 50  80  85  86  87  92 122]
    [-1. -1. -1.  6. -1. -1. -1.]
Non-Zero locations and entries in an interior edge-row:
    [258 283 287 288 289 293 318]
    [-1. -1. -1.  6. -1. -1. -1.]
Non-Zero locations and entries in an interior face-row:
    [800 824 829 830 831 836 860]
    [-1. -1. -1.  6. -1. -1. -1.]
Non-Zero locations and entries in an interior cell-row:
    [1243 1263 1267 1268 1269 1273 1293]
    [-1. -1. -1.  6. -1. -1. -1.]
```

and as can be seen, we get the stencils for $-\Delta$ again.

$$
\begin{bmatrix}
0&0&0&0&0&0&0&0&-\frac{1}{4}&-\frac{1}{4}&-\frac{1}{4}&0&0&0&0&0&0&0&0&0&0&0&0&0&0&0&0\\
0&0&0&0&0&0&0&0&\frac{1}{4}&0&0&-\frac{1}{4}&-\frac{1}{4}&0&0&0&0&0&0&0&0&0&0&0&0&0&0\\
0&0&0&0&0&0&0&0&0&\frac{1}{4}&0&0&0&-\frac{1}{4}&-\frac{1}{4}&0&0&0&0&0&0&0&0&0&0&0&0\\
0&0&0&0&0&0&0&0&0&0&0&\frac{1}{4}&0&\frac{1}{4}&0&-\frac{1}{4}&0&0&0&0&0&0&0&0&0&0&0\\
0&0&0&0&0&0&0&0&0&0&\frac{1}{4}&0&0&0&0&0&-\frac{1}{4}&-\frac{1}{4}&0&0&0&0&0&0&0&0&0\\
0&0&0&0&0&0&0&0&0&0&0&0&\frac{1}{4}&0&0&0&\frac{1}{4}&0&-\frac{1}{4}&0&0&0&0&0&0&0&0\\
0&0&0&0&0&0&0&0&0&0&0&0&0&0&\frac{1}{4}&0&0&\frac{1}{4}&0&-\frac{1}{4}&0&0&0&0&0&0&0\\
0&0&0&0&0&0&0&0&0&0&0&0&0&0&0&\frac{1}{4}&0&0&\frac{1}{4}&\frac{1}{4}&0&0&0&0&0&0&0\\
-\frac{1}{4}&\frac{1}{4}&0&0&0&0&0&0&0&0&0&0&0&0&0&0&0&0&0&0&\frac{1}{2}&-\frac{1}{2}&0&0&0&0&0\\
-\frac{1}{4}&0&\frac{1}{4}&0&0&0&0&0&0&0&0&0&0&0&0&0&0&0&0&0&-\frac{1}{2}&0&\frac{1}{2}&0&0&0&0\\
-\frac{1}{4}&0&0&0&\frac{1}{4}&0&0&0&0&0&0&0&0&0&0&0&0&0&0&0&0&\frac{1}{2}&-\frac{1}{2}&0&0&0&0\\
0&-\frac{1}{4}&0&\frac{1}{4}&0&0&0&0&0&0&0&0&0&0&0&0&0&0&0&0&\frac{1}{2}&0&0&\frac{1}{2}&0&0&0\\
0&-\frac{1}{4}&0&0&0&\frac{1}{4}&0&0&0&0&0&0&0&0&0&0&0&0&0&0&0&-\frac{1}{2}&0&-\frac{1}{2}&0&0&0\\
0&0&-\frac{1}{4}&\frac{1}{4}&0&0&0&0&0&0&0&0&0&0&0&0&0&0&0&0&-\frac{1}{2}&0&0&0&-\frac{1}{2}&0&0\\
0&0&-\frac{1}{4}&0&0&0&\frac{1}{4}&0&0&0&0&0&0&0&0&0&0&0&0&0&0&0&\frac{1}{2}&0&\frac{1}{2}&0&0\\
0&0&0&-\frac{1}{4}&0&0&0&\frac{1}{4}&0&0&0&0&0&0&0&0&0&0&0&0&0&0&0&\frac{1}{2}&-\frac{1}{2}&0&0\\
0&0&0&0&-\frac{1}{4}&\frac{1}{4}&0&0&0&0&0&0&0&0&0&0&0&0&0&0&0&\frac{1}{2}&0&0&0&\frac{1}{2}&0\\
0&0&0&0&-\frac{1}{4}&0&\frac{1}{4}&0&0&0&0&0&0&0&0&0&0&0&0&0&0&0&-\frac{1}{2}&0&0&-\frac{1}{2}&0\\
0&0&0&0&0&-\frac{1}{4}&0&\frac{1}{4}&0&0&0&0&0&0&0&0&0&0&0&0&0&0&0&-\frac{1}{2}&0&\frac{1}{2}&0\\
0&0&0&0&0&0&-\frac{1}{4}&\frac{1}{4}&0&0&0&0&0&0&0&0&0&0&0&0&0&0&0&0&\frac{1}{2}&-\frac{1}{2}&0\\
0&0&0&0&0&0&0&0&\frac{1}{2}&-\frac{1}{2}&0&\frac{1}{2}&0&-\frac{1}{2}&0&0&0&0&0&0&0&0&0&0&0&0&-1\\
0&0&0&0&0&0&0&0&-\frac{1}{2}&0&\frac{1}{2}&0&-\frac{1}{2}&0&0&0&\frac{1}{2}&0&0&0&0&0&0&0&0&0&-1\\
0&0&0&0&0&0&0&0&0&\frac{1}{2}&-\frac{1}{2}&0&0&0&\frac{1}{2}&0&0&-\frac{1}{2}&0&0&0&0&0&0&0&0&-1\\
0&0&0&0&0&0&0&0&0&0&0&\frac{1}{2}&-\frac{1}{2}&0&0&\frac{1}{2}&0&0&-\frac{1}{2}&0&0&0&0&0&0&0&1\\
0&0&0&0&0&0&0&0&0&0&0&0&0&-\frac{1}{2}&\frac{1}{2}&-\frac{1}{2}&0&0&0&\frac{1}{2}&0&0&0&0&0&0&1\\
0&0&0&0&0&0&0&0&0&0&0&0&0&0&0&0&\frac{1}{2}&-\frac{1}{2}&\frac{1}{2}&-\frac{1}{2}&0&0&0&0&0&0&1\\
0&0&0&0&0&0&0&0&0&0&0&0&0&0&0&0&0&0&0&0&-1&-1&-1&1&1&1&0
\end{bmatrix}
$$

Table A.1: Element Matrix in the 3D case.

Appendix B

Connection to the Dirac Operator from Physics

The Hodge-Dirac operator in 3D and the Dirac operator from physics are closely related, as elucidated by [11, Section 1.2], where the *complex* Dirac operator is considered

$$D_{\mathbb{C}} := \sum_{k=1}^{3} S_k \partial_k, \quad S_k := \begin{pmatrix} \mathbf{0}_{2\times 2} & \sigma_k \\ \sigma_k & \mathbf{0}_{2\times 2} \end{pmatrix} \in \mathbb{C}^{4\times 4},$$

where σ_k are the Pauli matrices

$$\sigma_1 = \begin{pmatrix} 0 & 1 \\ 1 & 0 \end{pmatrix}, \quad \sigma_2 = \begin{pmatrix} 0 & -i \\ i & 0 \end{pmatrix}, \quad \sigma_3 = \begin{pmatrix} 1 & 0 \\ 0 & -1 \end{pmatrix}.$$

By separating the real and imaginary parts of $D_{\mathbb{C}}$, applying permutations and swapping some signs, we get back to the Hodge-Dirac operator in 3D, see [21] or [11, Section 1.2] for an explicit computation.

It turns out that the Dirac equation for $\Psi(\mathbf{x}, t) \in \mathbb{C}^4$ (in $3+1$ dimensions) from physics can be written as

$$i\partial_t \Psi = -iD_{\mathbb{C}}\Psi + m \begin{pmatrix} 1 & & & \\ & 1 & & \\ & & -1 & \\ & & & -1 \end{pmatrix} \Psi, \tag{B.1}$$

see [10] for more. One could say that we are discretizing the spatial part of the momentum operator in (B.1) in this thesis.

There is also a formulation relying more on differential geometry, see [20] for more. The operator is of the form $d - \delta$, where d is the exterior derivative and δ the codifferential, so it looks similar to the Dirac operator, but with a different metric (signature $(+---)$ or $(-+++)$ depending on the convention), for which a similar discretization scheme to the ones considered in this thesis has been investigated in [4]. The reason why it is not possible to apply our techniques to that is that squaring this type of Dirac operator will lead to a (up to a sign) Laplacian *in the space-time metric*, hence it looks like a d'Alembert operator, which is unsuitable for designing a smoother.

Bibliography

[1] Robert Anderson et al. "MFEM: A modular finite element methods library". In: *Computers & Mathematics with Applications* 81 (Jan. 2021), pp. 42–74. ISSN: 0898-1221. DOI: 10.1016/j.camwa.2020.06.009.

[2] Douglas N. Arnold. *Finite Element Exterior Calculus*. Society for Industrial and Applied Mathematics, Dec. 2018. ISBN: 9781611975543. DOI: 10.1137/1.9781611975543.

[3] Ivo Babuška. "Error-bounds for finite element method". In: *Numerische Mathematik* 16.4 (Jan. 1971), pp. 322–333. ISSN: 0945-3245. DOI: 10.1007/bf02165003.

[4] P. Becher and H. Joos. "The Dirac-Kähler equation and fermions on the lattice". In: *Zeitschrift für Physik C Particles and Fields* 15.4 (Dec. 1982), pp. 343–365. ISSN: 1434-6052. DOI: 10.1007/bf01614426.

[5] A. Buffa and P. Ciarlet. "On traces for functional spaces related to Maxwell's equations Part I: An integration by parts formula in Lipschitz polyhedra". In: *Mathematical Methods in the Applied Sciences* 24.1 (2000), pp. 9–30. ISSN: 1099-1476. DOI: 10.1002/1099-1476(20010110)24:1<9::aid-mma191>3.0.co;2-2.

[6] Snorre H. Christiansen. "Foundations of Finite Element Methods for Wave Equations of Maxwell Type". In: *Applied Wave Mathematics*. Springer Berlin Heidelberg, 2009, pp. 335–393. ISBN: 9783642005855. DOI: 10.1007/978-3-642-00585-5_17.

[7] Snorre H. Christiansen, Hans Z. Munthe-Kaas, and Brynjulf Owren. "Topics in structure-preserving discretization". In: *Acta Numerica* 20 (Apr. 2011), pp. 1–119. ISSN: 1474-0508. DOI: 10.1017/s096249291100002x.

[8] M. Costabel, M. Dauge, and L. Demkowicz. "Polynomial extension operators for H^1, $\boldsymbol{H}(\mathbf{curl})$ and $\boldsymbol{H}(\mathbf{div})$-spaces on a cube". In: *Mathematics of Computation* 77.264 (Apr. 2008), pp. 1967–1999. ISSN: 0025-5718. DOI: 10.1090/s0025-5718-08-02108-x.

[9] Mathieu Desbrun et al. *Discrete Exterior Calculus*. 2005. DOI: 10.48550/ARXIV.MATH/0508341.

[10] Paul Adrien Maurice Dirac. "The quantum theory of the electron". In: *Proceedings of the Royal Society of London. Series A, Containing Papers of a Mathematical and Physical Character* 117.778 (Feb. 1928), pp. 610–624. ISSN: 2053-9150. DOI: 10.1098/rspa.1928.0023.

[11] Severin Fritschi. "Discontinuous Galerkin Method for Dirac and Curl Operators". MSc Thesis in CSE. D-MATH, ETH Zurich, 2023. URL: https://people.math.ethz.ch/~hiptmair/StudentProjects/Fritschi.Severin/Thesis_DG_Dirac_Curl.pdf.

[12] Johnny Guzmán and Pratyush Potu. *A Framework for Analysis of DEC Approximations to Hodge-Laplacian Problems using Generalized Whitney Forms*. 2025. arXiv: 2505.08934 [math.NA]. URL: https://arxiv.org/abs/2505.08934.

[13] Wolfgang Hackbusch. *Multi-Grid Methods and Applications*. Springer Berlin Heidelberg, 1985. ISBN: 9783662024270. DOI: 10.1007/978-3-662-02427-0.

[14] R. Hiptmair. "Discrete Hodge operators". In: *Numerische Mathematik* 90.2 (Dec. 2001), pp. 265–289. ISSN: 0945-3245. DOI: 10.1007/s002110100295.

[15] R. Hiptmair. "Finite elements in computational electromagnetism". In: *Acta Numerica* 11 (Jan. 2002), pp. 237–339. ISSN: 1474-0508. DOI: 10.1017/s0962492902000041.

[16] R. Hiptmair. "Operator Preconditioning". In: *Computers & Mathematics with Applications* 52.5 (Sept. 2006), pp. 699–706. ISSN: 0898-1221. DOI: 10.1016/j.camwa.2006.10.008. URL: http://dx.doi.org/10.1016/j.camwa.2006.10.008.

[17] Anil Nirmal Hirani. "Discrete exterior calculus". en. PhD thesis. 2003. DOI: 10.7907/ZHY8-V329.

[18] Masatoshi Kawai et al. "Parallel Smoother Based on Block Red-Black Ordering for Multigrid Poisson Solver". In: *High Performance Computing for Computational Science - VECPAR 2012*. Springer Berlin Heidelberg, 2013, pp. 292–299. ISBN: 9783642387180. DOI: 10.1007/978-3-642-38718-0_29.

[19] Paul Leopardi and Ari Stern. "The Abstract Hodge–Dirac Operator and Its Stable Discretization". In: *SIAM Journal on Numerical Analysis* 54.6 (Jan. 2016), pp. 3258–3279. ISSN: 1095-7170. DOI: 10.1137/15m1047684.

[20] Yu. N. Obukhov and S. N. Solodukhin. "Dirac equation and the Ivanenko-Landau-Kähler equation". In: *International Journal of Theoretical Physics* 33.2 (Feb. 1994), pp. 225–245. ISSN: 1572-9575. DOI: 10.1007/bf00844970.

[21] Rainer Picard, Sascha Trostorff, and Marcus Waurick. "On a connection between the Maxwell system, the extended Maxwell system, the Dirac operator and gravito-electromagnetism". In: *Mathematical Methods in the Applied Sciences* 40.2 (Dec. 2014), pp. 415–434. ISSN: 1099-1476. DOI: 10.1002/mma.3378.

[22] Erick Schulz and Gantumur Tsogtgerel. "Convergence of Discrete Exterior Calculus Approximations for Poisson Problems". In: *Discrete & Computational Geometry* 63.2 (Dec. 2019), pp. 346–376. ISSN: 1432-0444. DOI: 10.1007/s00454-019-00159-x.

[23] Matthew W. Scroggs et al. *DefElement: an encyclopedia of finite element definitions*. https://defelement.org. [Online; accessed 14-April-2025]. 2025.

[24] Denis Serre. *Matrices: Theory and Applications*. Springer New York, 2010. ISBN: 9781441976833. DOI: 10.1007/978-1-4419-7683-3.

[25] Evan VanderZee et al. "Well-Centered Triangulation". In: *SIAM Journal on Scientific Computing* 31.6 (Jan. 2010), pp. 4497–4523. ISSN: 1095-7197. DOI: 10.1137/090748214.

[26] Gabriel Wittum. "On the convergence of multi-grid methods with transforming smoothers: Theory with applications to the Navier-Stokes equations". In: *Numerische Mathematik* 57.1 (Dec. 1990), pp. 15–38. ISSN: 0945-3245. DOI: 10.1007/bf01386394.

[27] Sabine Zaglmayr. “High Order Finite Element Methodsfor Electromagnetic Field Computation”. PhD thesis. Johannes Kepler University Linz, 2006.

[28] Chengbin Zhu et al. *Convergence and Stability of Discrete Exterior Calculus for the Hodge Laplace Problem in Two Dimensions*. 2025. DOI: 10.48550/ARXIV.2505.08966.

Eidgenössische Technische Hochschule Zürich
Swiss Federal Institute of Technology Zurich

Declaration of originality

The signed declaration of originality is a component of every written paper or thesis authored during the course of studies. **In consultation with the supervisor**, one of the following two options must be selected:

☐ I hereby declare that I authored the work in question independently, i.e. that no one helped me to author it. Suggestions from the supervisor regarding language and content are excepted. I used no generative artificial intelligence technologies[1].

☒ I hereby declare that I authored the work in question independently. In doing so I only used the authorised aids, which included suggestions from the supervisor regarding language and content and generative artificial intelligence technologies. The use of the latter and the respective source declarations proceeded in consultation with the supervisor.

Title of paper or thesis:

MULTIGRID SOLVER FOR BOUNDARY VALUE PROBLEMS FOR THE DIRAC OPERATOR

Authored by:
If the work was compiled in a group, the names of all authors are required.

Last name(s):	**First name(s):**
Dabetic	Radovan

With my signature I confirm the following:
- I have adhered to the rules set out in the Citation Guidelines.
- I have documented all methods, data and processes truthfully and fully.
- I have mentioned all persons who were significant facilitators of the work.

I am aware that the work may be screened electronically for originality.

Place, date	**Signature(s)**
Wil SG, 11.09.2025	Radovan Dabetic

If the work was compiled in a group, the names of all authors are required. Through their signatures they vouch jointly for the entire content of the written work.

[1] For further information please consult the ETH Zurich websites, e.g. https://ethz.ch/en/the-eth-zurich/education/ai-in-education.html and https://library.ethz.ch/en/researching-and-publishing/scientific-writing-at-eth-zurich.html (subject to change).